

Aalto University
School of Science
Master's Programme in Engineering Physics

Miika Mäkelä

Mean-field studies of spin-imbalanced attractive Hubbard model in 1D and 2D quasicrystals

Master's Thesis
Espoo, October 22, 2018

Supervisor: Acad. Prof. Päivi Törmä

Advisor: PhD Long Liang

Author:	Miika Mäkelä	
Title:	Mean-field studies of spin-imbalanced attractive Hubbard model in 1D and 2D quasicrystals	
Date:	October 22, 2018	Pages: 60
Major:	Engineering Physics	Code: SCI3056
Supervisor:	Acad. Prof. Päivi Törmä	
Advisor:	PhD Long Liang	
<p>This thesis studies spin-imbalanced superconductivity in quasicrystals. Quasicrystals are structures that are ordered but not periodic. A familiar example of quasicrystals can be found in the Penrose tiling. Quasicrystals are characterized as structures that allow rotational symmetries that are not possible for periodic crystals. First quasicrystals were found in 1982, but superconductivity in quasicrystals was discovered only recently. The electronic behaviour of quasicrystals is well studied, at least in one dimension, but the effects of interactions in these complex systems have seen fairly few studies. Interactions, on the other hand, open a way to many interesting phenomena, such as superconductivity.</p> <p>In a superconducting material, electrons form Cooper pairs, which then carry the supercurrent. The main question is whether the typically forbidden rotational symmetries in quasicrystals enhance the pairing of electrons with finite momentum. This so called Fulde-Ferrel-Larkin-Ovchinnikov (FFLO) state is typically predicted to be stable when the two components that form the Cooper pair have different energies or, in other words, are spin-imbalanced.</p> <p>This thesis briefly presents the electronic properties of the non-interacting quasicrystals. The interactions between the electrons are described within the mean-field theory. The mean-field equations are solved iteratively in real space, the convergence of the iterations is studied, and the effect of the initial ansatz on the final state is discussed together with the results.</p> <p>The studied systems include a one-dimensional quasicrystal analogue, the Fibonacci chain, and a two dimensional tiling, the Ammann-Beenker tiling. The Fibonacci chain is found to support novel superconducting phases that reflect the aperiodic nature of the chain. The two-dimensional Ammann-Beenker tiling has eight-fold rotational symmetry and is found to support an oscillating phase with the same eight-fold rotational symmetry.</p>		
Keywords:	Bogoliubov-de-Gennes, superconductivity, quasicrystals	
Language:	English	

Tekijä:	Miika Mäkelä		
Työn nimi:	Keskeiskenttätutkimus epätasapainoisesta attraktiivisesta Hubbardin mallista yksi- ja kaksiulotteisissa kvasikristalleissa		
Päiväys:	22. lokakuuta 2018	Sivumäärä:	60
Pääaine:	Teknillinen Fysiikka	Koodi:	SCI3056
Valvoja:	Akatemiaprofessori Päivi Törmä		
Ohjaaja:	FT Long Liang		
<p>Tässä työssä tutkitaan suprajohtavuutta kvasikristalleissa. Kvasikristallit ovat rakenteita, jotka ovat säännöllisiä, mutta eivät toistuvia. Arkipäiväisimpiä esimerkkejä kvasikristalleista ovat erilaiset laatoitukset. Esimerkiksi Penrosen laatoitus on yleisesti käytetty kuvio katukivetyksissä. Ensimmäiset kvasikristallit löydettiin jo vuonna 1982, mutta kvasikristallien monimutkainen rakenne vaikeuttaa niitä kuvaavien teorioiden kehittämistä ja suuri osa teoreettisesta tutkimuksesta keskittyy yksiulotteisiin rakenteisiin. Vuorovaikuttavien hiukkasten käyttäytymistä kvasikristalleissa on tutkittu vain vähän ja ensimmäiset suprajohtavat kvasikristallit on löydetty vasta äskettäin.</p> <p>Suprajohtavassa materiaalissa aineen elektronit muodostavat Cooperin pareja, jotka ovat vastuussa häviöttömän supravirran kuljettamisesta. Työ keskittyy tutkimaan, miten kvasikristalleissa esiintyvät jaksollisille rakenteille kielletyt symmetriat vaikuttavat Cooperin parien muodostumiseen ja muodostavatko Cooperin parin todennäköisemmin elektronit eri energioilla, eli ovatko syntyvät parit spin-epätasapainoisia.</p> <p>Suprajohtavuutta kvasikristalleissa tutkitaan yksiulotteisessa Fibonaccin ketjussa ja kaksiulotteisen Ammann-Beenker laatoituksen avulla luodussa hilassa. Hiukkasten vuorovaikutuksia hilassa kuvataan keskeiskenttäteorian avulla. Työssä tarkastellaan yhtälöiden ratkaisemiseen käytettävien numeeristen menetelmien suppenemista ja erilaisten alkuyritteiden vaikutusta menetelmien tuottamiin ratkaisuihin. Yksiulotteisessa Fibonaccin ketjussa elektronien pariutumisen havaitaan noudattavan ketjun epäsäännöllistä rakennetta. Kaksiulotteinen Ammann-Beenker laatoitus on esimerkki rakenteesta, jolla on kahdeksankertainen rotaatio-symmetria. Tämä jaksollisille rakenteille mahdoton symmetria näkyy myös elektronien pariutumisessa.</p>			
Avainsanat:	Bogoliubov-de-Gennes, suprajohtavuus, kvasikristalli		
Kieli:	Englanti		

Acknowledgements

The completion of this thesis marks the end of five great years in Otaniemi. The completion of my studies in time is not an achievement I could have done by myself. I am lucky and grateful to have had an awesome group of friends from my initial freshmen group, *Denver Koloraato*, and I would like to specifically thank Tuomas, Olli, Neero, Jaarli, and Rasmus for being there to support and motivate me. In the beginning of my studies I also had an amazing group of friends from Guild of Cross, where I learned rules to countless board games.

For the large part of my studies the Guild of Physics has been the center of my free time. The guild has allowed me to meet countless people that are like-minded, willing to learn, excited, motivated, warm, and welcoming. I thoroughly enjoyed my time in the board the Guild of Physics, *Rairaati*, and I also owe a word of gratitude for them for support and friendship. At some point of my studies I started to miss playing volleyball, and I want to thank the people in Pus-Volley for all the volleyball games and practices.

I was able to work on this thesis in the Quantum Dynamics group, and I truly enjoyed the time spent working there. I want to thank everyone in the group who helped me complete my thesis, but especially Long Liang, who tirelessly answered my questions. Of course I want to thank my advisor Päivi Törmä who made the whole group atmosphere enjoyable and provided me with such an interesting topic.

To my mom and dad I want to say, thank you, for supporting my choices and always keeping me in their minds. My thanks also goes to my little brother Ilari, and our awesome cats. Of course I need to thank my uncle Tuomas for hinting at the possibility in studying Engineering Physics in the first place. I also want to thank my grandfather, Lauri Pippola, for always supporting my interest for mathematics. And finally I want to thank Emmi, for being my ultimate support.

Espoo, October 22, 2018

Miika Mäkelä

Contents

1	Introduction	6
1.1	Motivation	6
1.2	Structure of the thesis	7
2	Background	9
2.1	Quasicrystals	9
2.2	Fibonacci chain	12
2.3	Ammann-Beenker tiling	16
2.4	Tight-binding Hamiltonian	17
2.5	Bogoliubov-de-Gennes equations in real space	18
2.6	Grand canonical potential in real space	22
2.7	Self-consistent iteration	24
3	Results	29
3.1	Square lattice	29
3.2	Effects of the open boundary conditions	33
3.3	Pairing in Fibonacci chain	35
3.4	Fibonacci lattice	41
3.5	Pairing in Ammann-Beenker lattice	43
3.6	The LO phase in Ammann-Beenker lattice	45
4	Summary	49
A	Appendix	56
A.1	Fibonacci chain	57
A.2	Ammann-Beenker tiling	59

Chapter 1

Introduction

Motivation

Superconductivity was initially discovered in solid mercury at the temperature of 4 K (-269 °C) in 1911 by Heike Kamerlingh Onnes [1]. In a superconducting material electrical resistance goes to zero and magnetic fields are expelled from the material below a critical temperature T_c . The superconducting phenomenon in traditional superconductors was explained by Bardeen, Cooper, and Schrieffer in 1957 (BCS theory) [2]. In the BCS theory, electrons feel an effective attractive interaction and form Cooper pairs. The supercurrent is able to flow without dampening because resisting the supercurrent would require energy to break these Cooper pairs.

The first quasicrystals were discovered in 1982 in a rapidly cooled Al-Mn alloy by Dan Shechtman [3]. For his discovery, Dan Shechtman was awarded a Nobel prize in chemistry in 2011 [4]. The found material had a solid crystal structure and a diffraction pattern with a five fold rotational symmetry, forbidden for typical crystal structures. The found material had a definite long-range order but no periodicity. Soon after the initial discovery many other materials with similar properties were found [5, 6]. In practice, it is difficult to make a distinction between true quasicrystals and so called approximant quasicrystals which are periodic structures with large unit cells [7].

In the 1980's superconductivity was found in cuprates, that have critical temperatures as high as 133 K (-140 °C). The critical temperatures in cuprates are the highest known in atmospheric pressure [8]. It is now understood that in cuprates the pairing between electrons is more complex than in conventional BCS superconductors. However, the origin of the high critical temperatures is not yet completely understood [9]. Recently superconductiv-

ity similar to the cuprates was discovered in twisted bilayer graphene. This superconductivity emerges when one of the two layers of carbon atoms is slightly twisted with respect to the other layer and the carbon atoms become misaligned. This creates a structure with a large unit cell, similar to approximant quasicrystals [10].

To understand the interacting system of electrons in a quasicrystal, it is important to keep the non-interacting system in mind. Studies of the non-interacting systems have shown that the wave functions of quasicrystals are neither localised nor extended but rather critical [11]. Metal alloys can host either quasicrystalline or periodic phases, depending on the proportions of different elements in the alloy. Some alloys can be periodic in one direction but aperiodic in another direction, which can also make the electrical conductance dependent on the direction of the transport. In the alloy $\text{Al}_{65}\text{Cu}_{15}\text{Co}_{20}$, when the temperature is increased, the resistivity increases in the periodic plane but decreases in the quasiperiodic plane [12]. In general quasicrystals are poor conductors, but introducing defects to the quasiperiodic structure increases conductivity, showing that the small conductivity is mainly caused by the structure of quasicrystals [13].

Because of the lack of periodicity in quasicrystals, the most effective tools for understanding the behaviour of solids, Bloch theorem and Brillouin zones, cannot be used. The studies of superconductivity in quasicrystals then have to resort to real-space methods, such as the real-space dynamical mean-field theory, used in the study of pairing in the Penrose tiling [14]. There it was found that the pairing between different spin components follows the underlying lattice structure. Recent discovery of superconductivity in Al-Zn-Mg quasicrystals showed that quasicrystals can host superconductivity despite their complex electronic structure [15]. This thesis studies the possible superconducting phases in quasicrystals.

Structure of the thesis

Chapter 2 introduces the concept of a quasicrystal. What are the fundamental differences that make quasicrystals so different from normal crystals? Previous work on the subject is discussed and the different ways to obtain quasicrystals are introduced. Special attention is given to the one-dimensional analogue of a quasicrystal, the Fibonacci chain. This chapter also discusses the mean field equations that describe superconductivity in real space. The methods to solve these equations, along with limitations, are discussed.

Chapter 3 presents the results of the thesis. Initially the accuracy of the

used simulation model is confirmed by comparing to literature. The effect of the boundary conditions on the convergence of the iterative methods is studied. Following the investigation of the used methods, the focus turns to the different superconducting phases present in the Fibonacci chain. The Fibonacci chain is found to support four different phases, all of which show signs of the underlying aperiodic lattice. A lattice closer to real world quasicrystals, the Ammann-Beenker tiling, is studied to see whether these phases originate from the quasiperiodicity or are merely the effect of the exotic band structure of the Fibonacci chain. Finally, Chapter 4 presents the conclusions of this thesis.

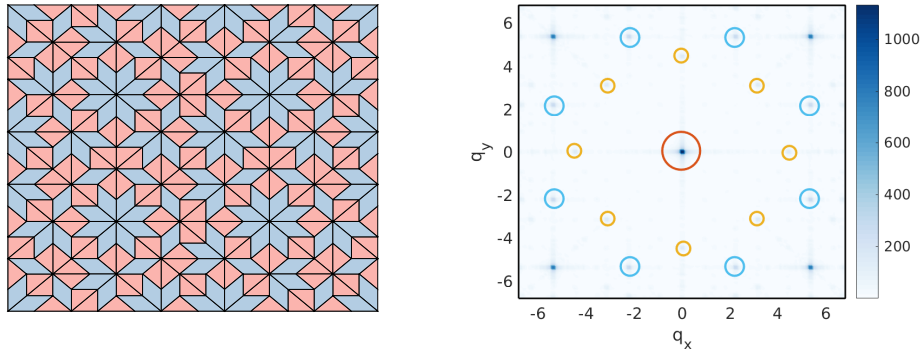
Chapter 2

Background

Quasicrystals

Most solid materials, such as metals, are well described by arrangement of atoms in lattice structures. The arrangements of atoms in periodic structures are restricted by the crystallographic restriction theorem. This theorem tells that periodic two-dimensional lattices can only have 2-, 3-, 4-, and 6-fold rotational symmetries. For example, a lattice with a three-fold rotational symmetry does not change when it is rotated by 60° about a rotation centre. In a periodic lattice there is at least one rotation centre for each unit cell [16]. Before the discovery of quasicrystals, well defined diffraction peaks were only met in periodic lattices. In 1982, Shechtman discovered a solid with a clear diffraction pattern that showed five-fold rotational symmetry, forbidden for periodic structures [3]. The clear diffraction pattern is a sign of long-range crystallographic order but the rotational symmetry of the diffraction tells that this structure cannot be periodic. The answer to such a dilemma is a structure that has long-range order but no periodicity, a quasicrystal.

The first found quasicrystal hosted an icosahedral phase, which is a phase with fivefold rotational symmetry, and it was found in a rapidly cooled Aluminum alloy [3]. Shortly after the initial discovery, a structure with twelvefold rotational symmetry was found in a NiCr alloy [5]. Since then, alloys with eightfold and tenfold rotational symmetries have also been found [17, 18] and currently over 100 quasicrystals are known [19]. Many quasicrystals produced in a laboratory are metastable and prepared with rapid solidification but some show stable quasicrystal phases, at least in high temperatures [18]. The first quasicrystal found to exist in nature was found northeast of Kamchatka Peninsula in Russia in 2009 and consists of mineral khatyrkite [20]. This mineral hosts an icosahedral phase and is composed of $\text{Al}_{65}\text{Cu}_{20}\text{Fe}_{15}$.



(a) Patch of the Ammann-Beenker tiling

(b) Absolute values of components of the Fourier transform of the lattice coordinates.

Figure 2.1: a) Ammann-Beenker tiling. b) The Fourier transform of the tiling. Largest peaks are marked with circles and the size of the circles represent the amplitudes of the peaks. The diffraction peaks show the eightfold rotational symmetry of the Ammann-Beenker tiling.

Quasicrystals are often found in alloys that contain Aluminum together and some transition metal. Depending on the relative occurrence of the different components in the alloy, the same alloy can also host periodic phases with either face- or body-centered cubic unit cells. Quasicrystals are in general poor conductors but those that contain transition metals have the largest resistivities. The resistivity in quasicrystals decreases with temperature, whereas in metals the resistivity increases with temperature. The same temperature dependence can also be seen in approximant quasicrystals. The resistivity of these alloys is the largest when they are closest to the perfect quasicrystalline structure [13, 18].

The essence of quasicrystals is well captured in different space filling tilings. Some of the most famous tilings are the Penrose [21] and the Ammann-Beenker tilings [22], with fivefold and eightfold rotational symmetries, respectively. An example of a patch of the Ammann-Beenker tiling is shown in Fig. 2.1a. In normal crystals, the rotational symmetries are restricted due to having many rotational centres, whereas in quasicrystals the rotational symmetries are not restricted but they can only have one centre of rotation. The rotational symmetry of a lattice or a tiling is therefore difficult to determine by only looking at the real space tiling. However, the Fourier transformed lattice clearly shows the rotational symmetries present in the lattice, as seen in Fig. 2.1b. Many tilings are aperiodic in two dimensions, but can be viewed as projections of periodic structures in higher dimensions [23]. For

example, the Penrose tiling is aperiodic in two dimensions, but can be projected into a two dimensional lattice from a periodic five-dimensional lattice. The Ammann-Beenker tiling and the Fibonacci chain can be projected from structures that are periodic in four and two dimensions, respectively. A more detailed description of obtaining aperiodic lattices with wanted symmetries through a projection is given in Ref. [23]. The projections from higher dimensions are not just a mathematical tool, but quasicrystals in one dimension can show boundary states and topological characteristics similar to the quantum Hall effect, usually found in two dimensions [24, 25].

In a periodic lattice the eigenstates of the non-interacting Hamiltonian are described by Bloch waves

$$\psi(\mathbf{x}) = u(\mathbf{x})e^{i\mathbf{k}\cdot\mathbf{x}}, \quad (2.1)$$

where $u(\mathbf{x})$ is a function that has the same periodicity as the lattice and \mathbf{k} is the lattice momentum. The eigenstates of this form can be found by taking advantage of the translational invariance of the lattice. Expanding the eigenstates as Bloch waves gives a direct relation between the momentum of the particle \mathbf{k} and the energy ε , resulting in a dispersion relation $\varepsilon(\mathbf{k})$. Without the translational invariance, the momentum of the particle cannot be directly related to its energy. To circumvent this, different schemes have been proposed. These schemes include relating the energies of the particles to a quasi-momentum [26] or calculating an effective dispersion relation [27].

The eigenstates of periodic systems are Bloch waves, but the form of the eigenstates of quasicrystals are not known in a general case. In a 1D quasiperiodic tight binding chain of fermions, the eigenfunctions of electrons decay with a power law and it is said that they are critical [28]. The structure of the quasicrystals is often self-similar, meaning that similar local environments are repeated and appear on different length scales. Different studies have suggested that also the non-interacting eigenstates of particles in a quasicrystals lattice reflect this self-similarity [29, 30]. This idea of similar local environments that dominate the eigenstates is reflected in one of the proposed ground states

$$\psi(\mathbf{i}) = C(\mathbf{i})e^{\kappa h(\mathbf{i})}, \quad (2.2)$$

where $C(\mathbf{i})$ is a site-dependent factor that is the same for lattice sites with similar environments and $h(\mathbf{i})$ is a height field that holds information about the underlying tiling. These eigenstates are referred to as Sutherland-Kalugin-Katz (SKK) eigenstates. It has been shown that the $E = 0$ state of the Fibonacci chain and the eigenstates of the Ammann-Beenker tiling have the SKK form [31, 32].

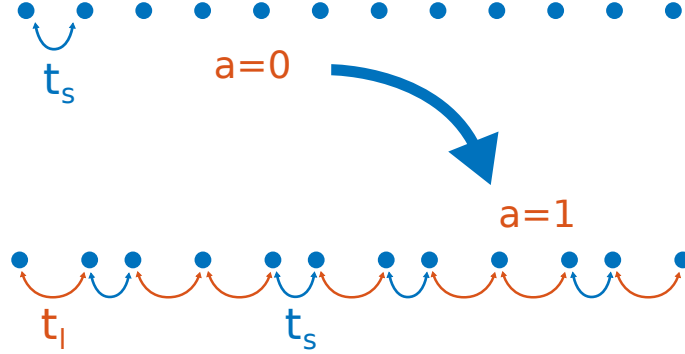


Figure 2.2: The change from a homogeneous chain of sites to a Fibonacci chain. The parameter a is used to describe how much the chain is changed. The hopping amplitude over short intervals t_s is kept constant. The long hopping amplitude over long intervals t_l is given by the parameter a as $t_l = e^{-a/\phi}$, where ϕ is the golden mean.

Fibonacci chain

The most studied one dimensional model of quasicrystals is the Fibonacci chain. This chain can be constructed straightforwardly with a set of string substitution rules

$$l \rightarrow ls, \quad (2.3)$$

$$s \rightarrow l. \quad (2.4)$$

The chain is created by starting with a letter l and applying the substitution rule repeatedly. For example, the five first strings will be

$$l \rightarrow ls \rightarrow lsl \rightarrow lslls \rightarrow lsllslls. \quad (2.5)$$

The lengths of the obtained strings form a Fibonacci series, hence the name of the chain. In a long chain, the ratio of the number of long intervals over the number of short intervals approaches an irrational number, the golden ratio $\phi = (\sqrt{5} + 1)/2$, giving the chain its aperiodic nature. The electronic spectrum of such a chain can be modelled with a simple tight-binding Hamiltonian [32]

$$H = \sum_i t_i \hat{c}_{i+1}^\dagger \hat{c}_i + H.c., \quad (2.6)$$

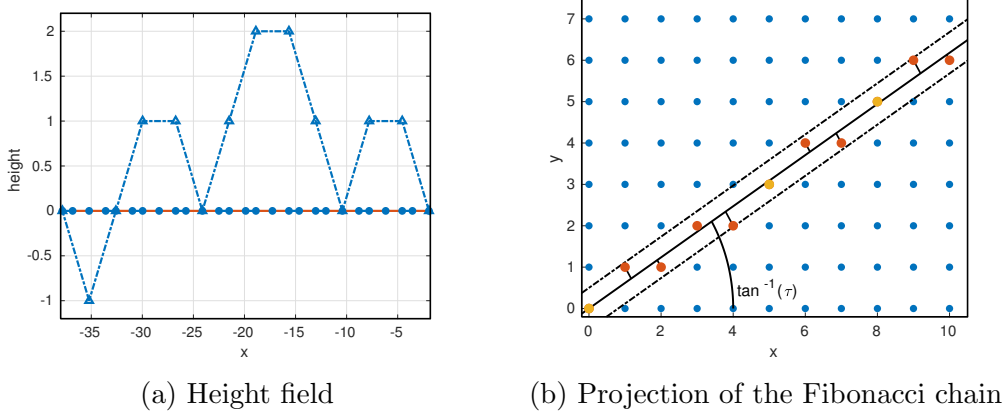


Figure 2.3: a) The blue and red lines denote short and long intervals, respectively. The height field is defined for a pair of intervals, see Eq. (2.7). b) The points within an acceptance domain are projected to a line. Sites closest to the line, marked as yellow, become the isolated sites.

where operator \hat{c}_i (\hat{c}_i^\dagger) annihilates (creates) a fermion at site i . The tunneling amplitudes t_i come from the letters of the Fibonacci string. The tunneling amplitudes between sites a short distance apart are denoted with $t_s = 1$ and a long distance apart with t_l , which is varied. The process is demonstrated in Fig. 2.2. The length of the short intervals are always 1 and the length of the long intervals is controlled with parameter a as $d_l = 1 + a\phi^{-1}$. With this choice, $a = 0$ is a uniform chain and $a = 1$ a Fibonacci chain where the distance between the long sites is ϕ . The hopping amplitudes between sites i and j are given by the exponential decay $t_{ij} = e^{1-|r_i-r_j|} = e^{-a/\phi}$. The tunneling amplitude between distant sites for $a = 1$ is $t_l = 0.53$. The different distances between the sites are only used for visualisation purposes and the actual behaviour of the Fibonacci chain is included in the tunneling amplitudes of the tight-binding Hamiltonian. This means that already for $a \neq 0$ the chain is a Fibonacci chain. The hopping amplitudes of the long intervals are given by an exponential function, but only nearest-neighbour tunnelings are considered.

The generated chain is aperiodic, but only has three distinct local environments. The first environment consists of a site that is a long distance away from both of its neighbouring sites. The two other local environments have one neighbour a short the other a long distance away. These three different environments can be seen in the spectrum of the tight-binding Hamiltonian (2.6) shown in 2.4. The longer range ordering of these local environments can be captured by a height field $h(i)$, formed from consecutive intervals [32]

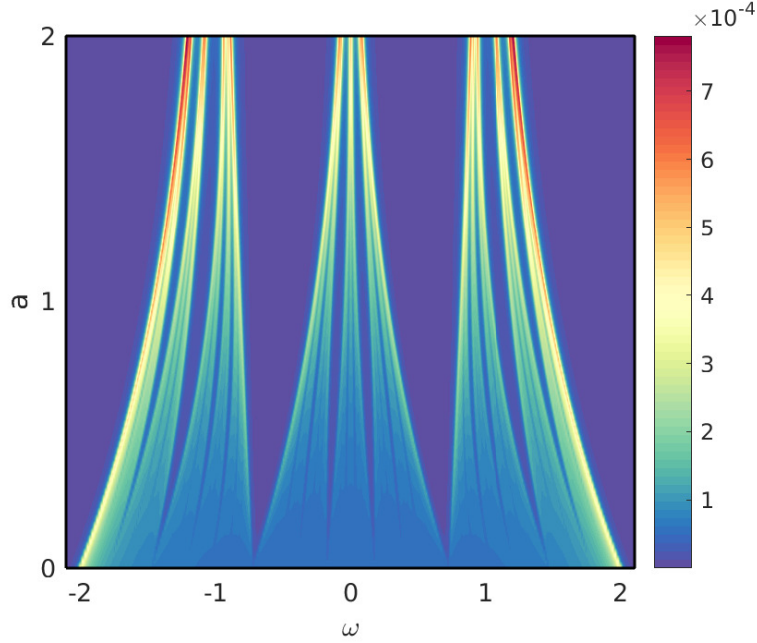


Figure 2.4: The density of states when moving from the square lattice towards the Fibonacci chain.

$$ls \rightarrow +1, \quad sl \rightarrow -1, \quad \text{and} \quad ll \rightarrow 0. \quad (2.7)$$

The height field generated in this way is shown in Fig. 2.3a. The height field constructed this way also corresponds to the height field in Eq. (2.2).

The substitution rule may be the most simple way to obtain the Fibonacci chain but another common way to obtain the chain is a so called cut and project (CP) method [7]. This method takes advantage of the fact that Fibonacci chain can be projected from a periodic lattice in two dimensions. The lattice points are then projected on a line with a slope τ . The points on the lattice are accepted if they are within a distance Ω from the line. When the slope of the line τ is irrational the obtained chain of points is quasiperiodic. Fibonacci chain is a special case of the projected points where the slope of the line is the inverse golden mean $\tau = (\sqrt{5} - 1)/2$. Comparing the CP method to the substitution rules, the slope determines the order of letters for the string and the offset in y -axis determines the initial starting letter the projection returns. Of course, for an infinite chain the initial letter is not important, but matters for a finite chain. The advantage of the CP methods is that they allow to obtain rational approximants of the chain. If the slope is $\tau = p/q$, where p and q are integers, a periodic approximant chain

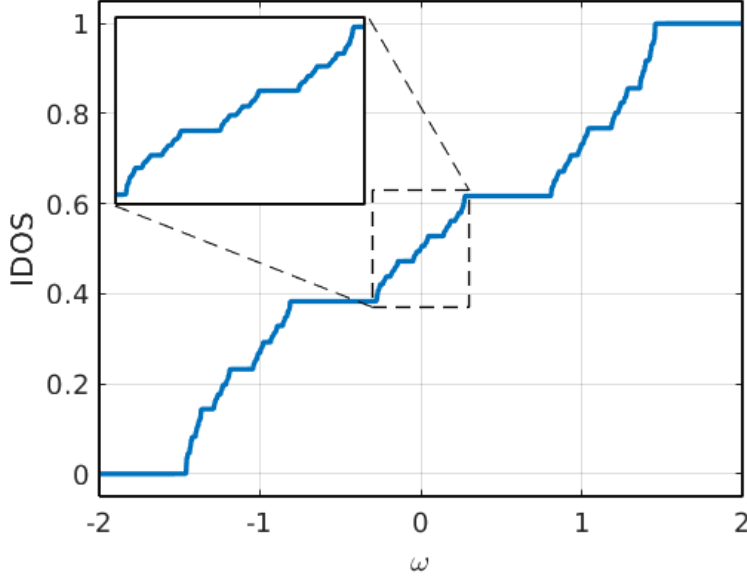


Figure 2.5: The integrated density of states of a Fibonacci chain with $N = 3 \cdot 10^4$ sites. The energy spectrum is given by the eigenenergies of the Hamiltonian in Eq. (2.6) with long hopping $t_l = -.53$. The inset shows the self-similar structure of the IDOS.

is obtained instead. The period of this approximant will be longer the closer the obtained ratio is to the actual golden ratio. CP method is a useful tool to gain intuition on the relation of the approximants and true quasicrystals.

Many quasicrystals and tilings are self-similar. Self-similarity means that the same patterns are repeated on multiple different scales. The self-similarity of the integrated density of states (IDOS) of a Fibonacci chain is shown in Fig. 2.5. The IDOS shows a large number of energy gaps, which retain their structure when looking at smaller and smaller energy intervals. One of the few exact results in regards to the electronic structure of quasicrystals is the gap labelling theorem (GLT) in one dimension. This theorem tells that inside an energy gap, the integrated density of states of a Fibonacci chain can only take certain values [32–34]

$$IDOS(\omega \in \text{gap}) = \frac{n}{1 + \alpha} \bmod 1, \quad (2.8)$$

where n is integer labelling the gap and α is the slope of the line that points from two dimensions are projected to. The Fibonacci chain is obtained when the parameter is the inverse golden mean $\alpha = \tau = (\sqrt{5} - 1)/2$.

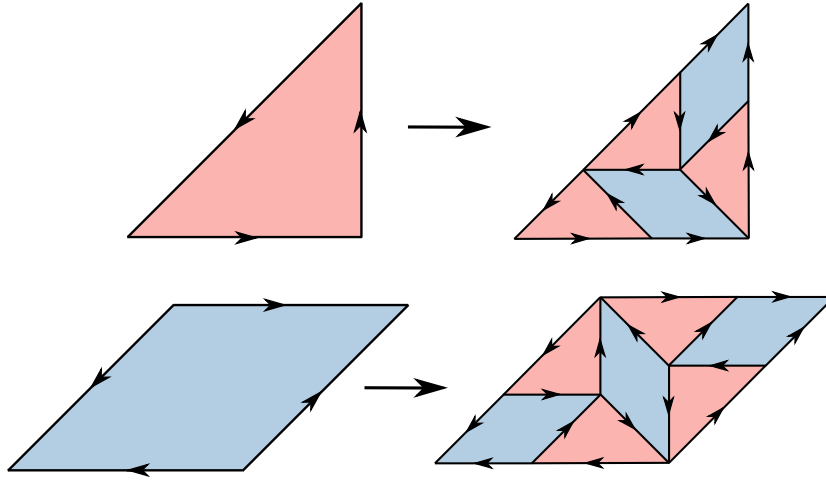


Figure 2.6: Substitution rules for the Ammann-Beenker A5 tiling.

Ammann-Beenker tiling

Ammann-Beenker tiling was introduced by Ammann in the 1970's and Beenker in 1982 [35], separately from each other [22]. The Ammann-Beenker tiling is a popular model for quasicrystals with eightfold rotational symmetry as it has nodes with eight connections to neighbouring nodes. The Ammann-Beenker tiling can be created either with a substitution rule applied consecutively on basic building blocks or as a projection of a four-dimensional hypercube to two dimensions. In this thesis a substitution rule is used. The substitution method inflates basic building blocks, a rhombus and a triangle. The inflations are started from a square that is constructed from two triangles. The substitution blocks are shown in Fig 2.6.

A neat way to see why the Ammann-Beenker tiling is aperiodic is based on the number of rhombi and squares on each iteration step. The number of the squares and rhombi at each inflation can be thought to increase as

$$\begin{bmatrix} N_r^{i+1} \\ N_t^{i+1} \end{bmatrix} = \begin{bmatrix} 3 & 2 \\ 4 & 3 \end{bmatrix} \begin{bmatrix} N_r^i \\ N_t^i \end{bmatrix} = M \begin{bmatrix} N_r^i \\ N_t^i \end{bmatrix} \quad (2.9)$$

When the number of iterations increases, the eigenvector corresponding to the largest eigenvalue of the M begins to dominate. The relation of the components of the eigenvector corresponds to the ratio of the number of squares and rhombi after many iterations. The ratio of $N_r^n/N_t^n \rightarrow 1/\sqrt{2}$ as $n \rightarrow \infty$. Because the ratio of the number of squares and rhombi is an irrational number, the tiling must be aperiodic [34].

Tight-binding Hamiltonian

Solving a full quantum-mechanical system for more than few components is not possible without a large computational effort. To overcome the difficulty of solving lattice systems with millions of sites some approximations are needed.

The first one will be a so called tight-binding approximation. In the tight-binding approximation the electrons are thought to be bound close to their host atoms and feel little effect of other atoms or electrons. In this lattice created by the host atoms, the electrons can move between the lattice sites by tunneling. Because electrons are fermions, only one electron can occupy one lattice site in a model with a single energy band. If the system has two different types of fermions, then a single lattice site can be occupied by two electrons of different type. The two different types of electrons are separated by an intrinsic angular momentum, spin. Only time the electrons interact, is when the two different spin components are at the same lattice site, a model known as the Hubbard model [36]. The common tight-binding Hamiltonian used to describe the possible electron energy states in the second quantized form is

$$\hat{H} = \sum_{\langle i,j \rangle, \sigma} t_{i,j} \hat{c}_{i\sigma}^\dagger \hat{c}_{j\sigma} - \sum_{i,\sigma} \mu_\sigma \hat{c}_{i\sigma}^\dagger \hat{c}_{i\sigma} + U \sum_i \hat{c}_{i\uparrow}^\dagger \hat{c}_{i\downarrow}^\dagger \hat{c}_{i\downarrow} \hat{c}_{i\uparrow}, \quad (2.10)$$

where indices i and j go over the lattice sites, $\langle \dots \rangle$ denotes a sum over the nearest neighbours, $t_{i,j}$ is the tunneling amplitude between sites i and j , μ_σ is the chemical potential of spin σ , and U the strength of the attractive interaction between the spin components. The operators $\hat{c}_{i\sigma}$ ($\hat{c}_{i\sigma}^\dagger$) annihilate (create) a fermion with spin $\sigma = \uparrow, \downarrow$ on lattice site i .

The first term in the Hamiltonian describes the tunneling between lattice sites. The term destroys a fermion on the current lattice site and creates a fermion on a neighbouring site. The tunneling amplitudes are thought to be significant only between the nearest neighbour lattice sites. This, kinetic or hopping Hamiltonian, term captures the essence of the lattice geometry and gives the possible non-interacting energy eigenstates of the lattice.

The second term in the Hamiltonian gives the spins a chemical potential and is given relative to the number of fermions on the site $\hat{n}_{i\sigma} = \hat{c}_{i\sigma}^\dagger \hat{c}_{i\sigma}$. By tuning the chemical potential, the occupied energy state of the spin component can be changed. This allows the investigation of the behaviour of the system when the two spin components occupy different energy states.

The third term describes the interaction between the two spin components. It depends on the number of both spin components on the site i .

The interaction term can be simplified with a mean-field approximation $U\hat{c}_{i\uparrow}^\dagger\hat{c}_{i\downarrow}^\dagger\hat{c}_{i\downarrow}\hat{c}_{i\uparrow} \approx \hat{c}_{i\uparrow}^\dagger\hat{c}_{i\downarrow}^\dagger\Delta_i + \Delta_i^*\hat{c}_{i\downarrow}\hat{c}_{i\uparrow} - \frac{|\Delta_i|^2}{U}$, where $\Delta_i = U\langle\hat{c}_{i\downarrow}\hat{c}_{i\uparrow}\rangle$

$$\hat{H} = \sum_{\langle i,j \rangle, \sigma} t_{i,j}\hat{c}_{i\sigma}^\dagger\hat{c}_{j\sigma} - \sum_{i,\sigma} \mu_\sigma\hat{c}_{i\sigma}^\dagger\hat{c}_{i\sigma} + \sum_i \left(\hat{c}_{i\uparrow}^\dagger\hat{c}_{i\downarrow}^\dagger\Delta_i + \Delta_i^*\hat{c}_{i\downarrow}\hat{c}_{i\uparrow} - \frac{|\Delta_i|^2}{U} \right). \quad (2.11)$$

Here the parameter Δ_i tells the pairing amplitude of the different spin components at site i and it is the order parameter of the BCS phase. A non-zero Δ tells that the electrons form Cooper pairs and the system is superconducting. When the order parameter is zero the system is in a normal state. Whether the system has non-zero BCS order parameter is determined by comparing the energies of the system both in the BCS state and the normal state. In this thesis the system is studied with varying chemical potentials μ_σ . The two chemical potentials are combined into the average chemical potential

$$\mu = \frac{\mu_\uparrow + \mu_\downarrow}{2}, \quad (2.12)$$

and the effective magnetic field, the difference of the chemical potentials

$$h = \frac{\mu_\uparrow - \mu_\downarrow}{2}. \quad (2.13)$$

The name effective magnetic field comes from the fact that applying an external magnetic field changes the energy of a particle with spin $\Delta E_B = \mu\mathbf{B} \cdot \mathbf{h}$. This imbalance in the chemical potentials of the different spins can make a phase where the Cooper pairs form with a momentum \mathbf{q} favourable. This type of a phase was first proposed by Larkin and Ovchinnikov (LO) [37] and Fulde and Ferrel (FF) [38] independently. In the FF phase the order parameter oscillates with a phase $\Delta = \Delta_0 e^{i\mathbf{q} \cdot \mathbf{r}}$ and in the LO phase the order parameter oscillates with amplitude $\Delta = \Delta_0 \cos(\mathbf{q} \cdot \mathbf{r})$. The formation of such a phase is typically explained with the matching of the different Fermi surfaces with a wavevector \mathbf{q} in the momentum space. This explanation is illustrated in Fig. 2.7 for a one dimensional chain.

Bogoliubov-de-Gennes equations in real space

To solve the energies of the system, the problem is transformed into a matrix form. The eigenstates then give the possible energy states the system can have. The matrix form of the equation (2.11) are commonly known as the Bogoliubov-de-Gennes (BdG) Hamiltonian. BdG Hamiltonian is most

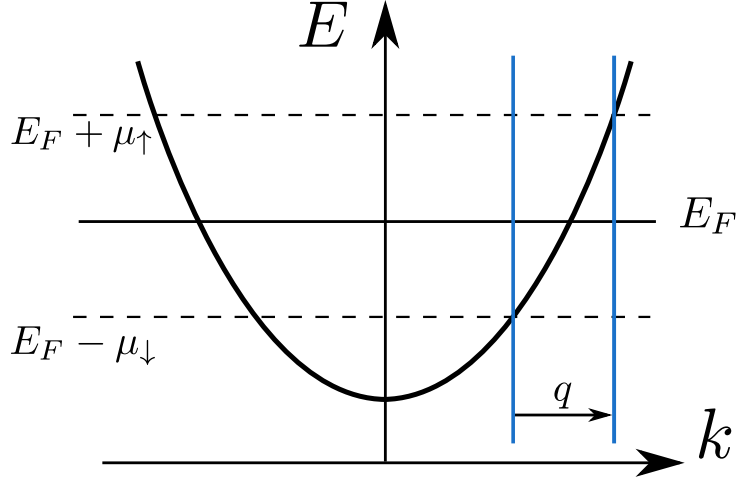


Figure 2.7: The dispersion of a one dimensional uniform tight-binding chain. The Fermi levels of different components are shifted by their chemical potentials. When the difference of the Fermi levels increases, it is energetically favourable to form pairs with finite momentum q . In real space this leads to an oscillating order parameter $\Delta = \Delta_0 \cos(qr)$ (LO) or $\Delta = \Delta_0 e^{iqr}$ (FF).

commonly used when simulating real-space impurities, spin-imbanced superfluids or when the lattice lacks translational symmetry [39] [40]. BdG Hamiltonian consists of two diagonal blocks $H - \mu_\sigma$, that describe the single particle energies of the two spin components. The sign of the lower diagonal block has been swapped due to the anti-commutation of the fermionic operators on the assembly stage of the matrix. The off-diagonal blocks Δ describe the interactions between the two distinct species. The creation and annihilation operators for individual sites have been gathered into a single vector $[\hat{c}_\uparrow \ \hat{c}_\downarrow]^T = [\hat{c}_{1\uparrow} \dots \hat{c}_{n\uparrow} \ \hat{c}_{1\downarrow} \dots \hat{c}_{n\downarrow}]^T$ and the Hamiltonian in this basis becomes

$$\hat{H} = \begin{bmatrix} \hat{c}_\uparrow^\dagger & \hat{c}_\downarrow \end{bmatrix} \begin{bmatrix} H_t - \mu_\uparrow & \Delta \\ \Delta & -H_t + \mu_\downarrow \end{bmatrix} \begin{bmatrix} \hat{c}_\uparrow \\ \hat{c}_\downarrow \end{bmatrix} + C, \quad (2.14)$$

where C is a constant. The size of the single particle Hamiltonian H is $n \times n$, where n is the number of lattice sites. The size of the total Hamiltonian is thus $2n \times 2n$. As can be seen, this Hamiltonian is not diagonal in the basis of the single lattice site annihilation (creation) operators \hat{c} (\hat{c}^\dagger). To obtain the physics of the interacting system, one needs to transform the Hamiltonian into a basis of quasiparticle annihilation (creation) operators $\hat{\gamma}$ ($\hat{\gamma}^\dagger$). A basis in which the Hamiltonian is diagonal is the energy eigenbasis

for the interacting system. The interactions between particles are hidden inside the definition of quasiparticles, and the quasiparticles themselves are thought as noninteracting. The Hamiltonian can be diagonalized by inserting unitary matrices $\mathbb{1} = \mathcal{W}\mathcal{W}^\dagger$

$$H = \hat{c}^\dagger \mathcal{W} \mathcal{W}^\dagger H \mathcal{W} \mathcal{W}^\dagger \hat{c} + C = \hat{\gamma}^\dagger E \hat{\gamma} + C, \quad (2.15)$$

where \mathcal{W} is a unitary matrix that contains the eigenvectors of the Hamiltonian. Matrix E is a diagonal matrix that contains the eigenvalues of the system, fulfilling the equation

$$H\mathcal{W} = \mathcal{W}E. \quad (2.16)$$

The quasiparticle annihilation (creation) operators are connected to the lattice annihilation (creation) operators through the unitary matrix \mathcal{W}

$$\hat{c} = \mathcal{W}\hat{\gamma} \quad \text{and} \quad \hat{c}^\dagger = \hat{\gamma}^\dagger \mathcal{W}^\dagger. \quad (2.17)$$

Respecting the original structure of the lattice operator, the quasiparticle operators can also be divided into two components by writing the unitary matrix \mathcal{W} as a block matrix

$$\begin{bmatrix} \hat{c}_\uparrow \\ \hat{c}_\downarrow \end{bmatrix} = \begin{bmatrix} A & B \\ C & D \end{bmatrix} \begin{bmatrix} \hat{\gamma}_\uparrow \\ \hat{\gamma}_\downarrow \end{bmatrix}. \quad (2.18)$$

this allows us to connect the annihilation operator for site i to the elements of the unitary transform

$$\hat{c}_{i\uparrow} = \sum_{j=1}^n (A_{i,j} \hat{\gamma}_{j\uparrow} + B_{i,j} \hat{\gamma}_{j\downarrow}^\dagger). \quad (2.19)$$

The operator $\hat{c}_{i\downarrow}$ can be formulated similarly and the order parameter $\Delta_i = U \langle \hat{c}_{i\downarrow} \hat{c}_{i\uparrow} \rangle$ becomes

$$\begin{aligned} \langle \hat{c}_{i\downarrow} \hat{c}_{i\uparrow} \rangle &= \left\langle \left(\sum_{k=1}^n C_{i,k}^* \hat{\gamma}_{k\uparrow}^\dagger + D_{i,k}^* \hat{\gamma}_{k\downarrow} \right) \left(\sum_{j=1}^n A_{i,j} \hat{\gamma}_{j\uparrow} + B_{i,j} \hat{\gamma}_{j\downarrow}^\dagger \right) \right\rangle = \\ & \sum_{(j,k)=1}^n C_{i,k}^* A_{i,j} \langle \hat{\gamma}_{k\uparrow}^\dagger \hat{\gamma}_{j\uparrow} \rangle + D_{i,k}^* A_{i,j} \langle \hat{\gamma}_{k\downarrow} \hat{\gamma}_{j\uparrow} \rangle + C_{i,k}^* B_{i,j} \langle \hat{\gamma}_{k\uparrow}^\dagger \hat{\gamma}_{j\downarrow}^\dagger \rangle + D_{i,k}^* B_{i,j} \langle \hat{\gamma}_{k\downarrow} \hat{\gamma}_{j\downarrow} \rangle. \end{aligned} \quad (2.20)$$

Within the BCS-theory, the expectation values $\langle \hat{\gamma}_{k\downarrow} \hat{\gamma}_{j\uparrow} \rangle = 0$ and $\langle \hat{\gamma}_{k\uparrow} \hat{\gamma}_{j\downarrow} \rangle = 0$. As noted previously, the quasiparticles are noninteracting and the expectation values $\langle \hat{\gamma}_j^\dagger \hat{\gamma}_i \rangle = \langle \hat{\gamma}_j^\dagger \hat{\gamma}_i \rangle \delta_{i,j}$. The expression for the order parameter is simplified to

$$\langle \hat{c}_{i\downarrow} \hat{c}_{i\uparrow} \rangle = \sum_{j=1}^n C_{i,j}^* A_{i,j} \langle \hat{\gamma}_{j\uparrow}^\dagger \hat{\gamma}_{j\uparrow} \rangle + D_{i,j}^* B_{i,j} \langle \hat{\gamma}_{j\downarrow} \hat{\gamma}_{j\downarrow}^\dagger \rangle. \quad (2.21)$$

The quasiparticle operators were obtained from the single-particle operators through unitary transformation which guarantees that they still obey Fermi-statistics. The expectation values $\langle \hat{\gamma}_{j\uparrow}^\dagger \hat{\gamma}_{j\uparrow} \rangle$ are given by the Fermi-Dirac distribution $n_F(E, T) = 1/(e^{\beta E} + 1)$, where $\beta = 1/(k_B T)$ is the inverse of temperature times the Boltzmann constant. In the second term of Eq. (2.21) the creation and annihilation operators seem to have the wrong order. This problem is alleviated if one takes a look at the quasiparticle energies

$$\hat{H} = \begin{bmatrix} \hat{\gamma}_\uparrow^\dagger & \hat{\gamma}_\downarrow \end{bmatrix} \begin{bmatrix} E_\uparrow & 0 \\ 0 & E_\downarrow \end{bmatrix} \begin{bmatrix} \hat{\gamma}_\uparrow \\ \hat{\gamma}_\downarrow^\dagger \end{bmatrix} = \sum_i \hat{\gamma}_{i\uparrow}^\dagger \hat{\gamma}_{i\uparrow} E_{i\uparrow} + \hat{\gamma}_{i\downarrow} \hat{\gamma}_{i\downarrow}^\dagger E_{i\downarrow}, \quad (2.22)$$

where the order of the operators for the down components is the same as in Eq. (2.21). Because of this it is possible to directly insert the Fermi-Dirac distributions and obtain

$$\hat{H} = \sum_{j=1}^n C_{i,j}^* A_{i,j} n_F(E_{j\uparrow}, T) + D_{i,j}^* B_{i,j} n_F(E_{j\downarrow}, T). \quad (2.23)$$

The order parameter can actually be simply denoted with

$$\Delta_i = U \langle \hat{c}_{i\downarrow} \hat{c}_{i\uparrow} \rangle = U \sum_j^{2n} \mathcal{W}_{i,j} \mathcal{W}_{i+n,j}^* n_F(E_j, T), \quad (2.24)$$

where the structure of the matrix \mathcal{W} was used to combine the two different blocks. The order parameter is thus governed by a single equation that restricts the possible values the order parameter can have. Thus to solve the state of the system one needs to see whether the order parameter fulfills this self-consistent condition.

In addition to the order parameter, an important quantity is the density of different components on each lattice site. Similar to the order parameter the density at each site can be calculated through the components of the matrix \mathcal{W} . The up component density $n_\uparrow = \langle \hat{n}_\uparrow \rangle = \langle \hat{c}_{i\uparrow}^\dagger \hat{c}_{i\uparrow} \rangle$ can be obtained as

$$\begin{aligned}
n_{i\uparrow} &= \langle \hat{c}_{i\uparrow}^\dagger \hat{c}_{i\uparrow} \rangle = \left\langle \left(\sum_j^n A_{i,j}^* \hat{\gamma}_{j\uparrow}^\dagger + B_{i,j}^* \hat{\gamma}_{j\downarrow} \right) \left(\sum_k^n A_{i,k} \hat{\gamma}_{k\uparrow} + B_{i,k} \hat{\gamma}_{k\downarrow}^\dagger \right) \right\rangle \\
&= \sum_j A_{i,j} A_{i,j}^* \langle \hat{\gamma}_{j\uparrow}^\dagger \hat{\gamma}_{j\uparrow} \rangle + B_{i,j} B_{i,j}^* \langle \hat{\gamma}_{j\downarrow} \hat{\gamma}_{j\downarrow}^\dagger \rangle = \sum_j^{2n} \mathcal{W}_{i,j} \mathcal{W}_{i,j}^* n_F(E_j, T). \quad (2.25)
\end{aligned}$$

Again the ordering of the operators in the second term allows the direct insertion of the Fermi-Dirac distributions. For the density of the down component the operators need to be commuted

$$\begin{aligned}
n_{i\downarrow} &= \langle \hat{c}_{i\downarrow}^\dagger \hat{c}_{i\downarrow} \rangle = \left\langle \left(\sum_j^n C_{i,j} \hat{\gamma}_{j\uparrow} + D_{i,j} \hat{\gamma}_{j\downarrow}^\dagger \right) \left(\sum_k^n C_{i,k}^* \hat{\gamma}_{k\uparrow}^\dagger + D_{i,k} \hat{\gamma}_{k\downarrow} \right) \right\rangle \\
&= \sum_j^n C_{i,j} C_{i,j}^* \langle \hat{\gamma}_{j\uparrow} \hat{\gamma}_{j\uparrow}^\dagger \rangle + D_{i,j} D_{i,j}^* \langle \hat{\gamma}_{j\downarrow}^\dagger \hat{\gamma}_{j\downarrow} \rangle \\
&= \sum_j^n C_{i,j} C_{i,j}^* (1 - \langle \hat{\gamma}_{j\uparrow}^\dagger \hat{\gamma}_{j\uparrow} \rangle) + D_{i,j} D_{i,j}^* (1 - \langle \hat{\gamma}_{j\downarrow} \hat{\gamma}_{j\downarrow}^\dagger \rangle) \\
&= \sum_j^n C_{i,j} C_{i,j}^* (1 - n_F(E_{j\uparrow}, T)) + D_{i,j} D_{i,j}^* (1 - n_F(E_{j\downarrow}, T)) \\
&= \sum_j^{2n} \mathcal{W}_{i+n,j} \mathcal{W}_{i+n,j}^* (1 - n_F(E_j, T)) = \sum_j^{2n} \mathcal{W}_{i+n,j} \mathcal{W}_{i+n,j}^* n_F(-E_j, T), \quad (2.26)
\end{aligned}$$

where the property $1 - n_F(E, T) = n_F(-E, T)$ was used on the last line. Subsequently the polarization of the lattice will be calculated as the difference of the average densities of two spin components.

Grand canonical potential in real space

This section briefly goes through the derivation of the grand potential for a real space calculation. This closely follows the derivation in \mathbf{k} -space found in the dissertation of Koponen [41]. Starting from equation (2.22) with all the constant terms explicitly written the Hamiltonian for the real space lattice is

$$\hat{H} = \sum_i \left(\hat{\gamma}_{i\uparrow}^\dagger \hat{\gamma}_{i\uparrow} E_{i\uparrow} + (1 - \hat{\gamma}_{i\downarrow}^\dagger \hat{\gamma}_{i\downarrow}) E_{i\downarrow} - \frac{|\Delta_i|^2}{U} - \mu_\downarrow + H_{\downarrow ii} \right). \quad (2.27)$$

The partition function of the system is written as

$$\mathcal{Z} = \text{Tr}\{e^{-\beta\hat{H}}\}. \quad (2.28)$$

The trace can be taken over any complete basis of the system. One benefit of the diagonalization of the BdG Hamiltonian is that the trace is now easier to take over the quasiparticle states $|\gamma\rangle$. In this basis, the last three terms in Eq. (2.27) are constants and will be included in $C = \sum_i \left(-\frac{|\Delta_i|^2}{U} - \mu_\downarrow + H_{\downarrow ii} \right)$.

Expanding the partition function

$$\begin{aligned} \mathcal{Z} &= \text{Tr}\{e^{-\beta C} e^{-\beta \sum_i E_{i\uparrow} \hat{\gamma}_{i\uparrow}^\dagger \hat{\gamma}_{i\uparrow} + (1 - \hat{\gamma}_{i\downarrow}^\dagger \hat{\gamma}_{i\downarrow}) E_{i\downarrow}}\} \\ &= e^{-\beta C} \sum_\gamma \langle \gamma | e^{-\beta \sum_i E_{i\uparrow} \hat{\gamma}_{i\uparrow}^\dagger \hat{\gamma}_{i\uparrow} + (1 - \hat{\gamma}_{i\downarrow}^\dagger \hat{\gamma}_{i\downarrow}) E_{i\downarrow}} | \gamma \rangle, \end{aligned} \quad (2.29)$$

where sum over γ goes through all the quasiparticle states. The sum over the sites i can be taken out of the exponent as a product of the exponents and the quasiparticle operators can be replaced with the number operators $\hat{n}_{i\uparrow} = \hat{\gamma}_{i\uparrow}^\dagger \hat{\gamma}_{i\uparrow}$

$$\mathcal{Z} = e^{-\beta C} \sum_\gamma \langle \gamma | \prod_i e^{-\beta E_{i\uparrow} \hat{n}_{i\uparrow}} e^{-\beta E_{i\downarrow} (1 - \hat{n}_{i\downarrow})} | \gamma \rangle. \quad (2.30)$$

The current basis is the eigenbasis of the number operators of quasiparticles and by operating on the basis $e^{-\beta E_{i\sigma} \hat{n}_{i\sigma}} |\gamma\rangle = e^{-\beta E_{i\sigma} n_{i\sigma}} |\gamma\rangle$, where $n_{i\sigma}$ is the number of particles with spin σ at site i . And since $\langle \gamma | \gamma \rangle = \mathbb{1}$,

$$\mathcal{Z} = e^{-\beta C} \sum_\gamma \prod_i e^{-\beta E_{i\uparrow} n_{i\uparrow\gamma}} e^{-\beta E_{i\downarrow} (1 - n_{i\downarrow\gamma})}. \quad (2.31)$$

Here it is possible to change the order of the product over lattice sites and the sum over the quasiparticle states

$$\mathcal{Z} = e^{-\beta C} \prod_i \sum_{n_{\uparrow\gamma}} e^{-\beta E_{i\uparrow} n_{i\uparrow\gamma}} \sum_{n_{\downarrow\gamma}} e^{-\beta E_{i\downarrow} (1 - n_{i\downarrow\gamma})}. \quad (2.32)$$

The quasiparticle operators are fermionic and the $n_{i\sigma\gamma} \in \{0, 1\}$

$$\mathcal{Z} = e^{-\beta C} \prod_i (e^{-\beta \cdot 0} + e^{-\beta E_{i\uparrow} \cdot 1}) (e^{-\beta E_{i\downarrow} (1-0)} + e^{-\beta E_{i\downarrow} (1-1)}), \quad (2.33)$$

$$= e^{-\beta C} \prod_i (1 + e^{-\beta E_{i\uparrow}}) (e^{-\beta E_{i\downarrow}} + 1). \quad (2.34)$$

The grand potential is given by

$$\Omega = -\frac{1}{\beta} \ln(\mathcal{Z}). \quad (2.35)$$

Taking the logarithm of the partition function results in the final form for the grand potential

$$\Omega = \sum_i \left(-\frac{|\Delta_i|^2}{U} - \mu_{\downarrow} + H_{\downarrow ii} \right) - \frac{1}{\beta} \sum_i \ln(1 + e^{-\beta E_{i\uparrow}}) + \ln(e^{-\beta E_{i\downarrow}} + 1). \quad (2.36)$$

It is now clear that the distinction of the quasiparticle energies to up- and down-components has no effect on the final grand potential. The final grand potential also has contribution from the diagonal terms of the tight-binding Hamiltonian, $H_{\downarrow ii}$, which can be understood as an energy offset of the i :th site.

Self-consistent iteration

As noticed in Section 2.5 the order parameter Δ can be calculated by diagonalising the BdG Hamiltonian (Eq. (2.14)). But inserting this solution back into the original BdG matrix returns a new matrix, different from the initial one. This step of solving the order parameter and then inserting the solution back into the original matrix is one self-consistent iteration. By repeating this process, the matrix converges to a solution that is an actual solution for the initial problem. The downside of the self-consistent iteration is that the initial ansatz for the order parameter Δ has a significant effect on the converged solution. The convergence towards the final solution can also be slow, especially for large lattices.

There exists a large amount of literature about the self-consistent iterations, also for spin-imbalanced systems [39, 40]. The self-consistent iteration procedure can also be seen as a minimization problem, and different approaches to obtain faster convergence show similar traits to the solutions of minimization problems. The steps to solve the order parameter self-consistently at iteration $m + 1$ are included in a function g

$$\Delta^{(m+1)} = g(H_{\text{BdG}}(\Delta^{(m)})). \quad (2.37)$$

After calculating the new order parameter, the order parameter is inserted back into the original Bogoliubov-de-Gennes Hamiltonian H_{BdG} . The process is then repeated until the relative error of the order parameter is below a threshold or the maximum number of iterations is reached.

The convergence of the self-consistent iteration procedure has been studied in great amounts, but due to the richness and complexity of the problem, no general guarantees of convergence or finding a global minimum are given [42]. The convergence of the iterations can be increased by mixing subsequent order parameters

$$\Delta^{(m+1)} = (1 - w)\Delta^{(m)} + w \cdot g(H_{\text{BdG}}(\Delta^{(m)})) \quad (2.38)$$

where the factor $w \in]0, 1]$ determines the weight between the subsequent Δ . One of the slightly more complicated methods is Broyden's method [43], which was later improved by Johnson [44]. The improved method has been used in electronic structure calculations [45] and in the study of coexistence of different phases in Fermi gases [39, 40]. Broyden's method takes advantage of the idea of mixing the subsequent iteratives in a way to decrease the error of the new iterative. Broyden updates the variables in a quasi-Newton step

$$\Delta^{(m+1)} = \Delta^{(m)} + G^{(m)} F^{(m)}, \quad (2.39)$$

where $F^{(m)} = g(\Delta^{(m)}) - \Delta^{(m)}$ is the difference between the current Δ and the one obtained from the self-consistent function evaluation of $g(\Delta)$. For a result to converge, F should thus decrease with iteration steps. By requiring that the difference between adjacent update matrices $|G^{(m+1)} - G^{(m)}|$ is minimized, an update equation follows

$$G^{(m+1)} = G^{(m)} - (\delta\Delta^{(m)} + G^{(m)}\delta F^{(m)})\delta F^{(m)}. \quad (2.40)$$

Initially matrix G can be set to unity. The changes in Δ and F are normalized to unit length

$$\delta\Delta^{(m)} = \frac{\Delta^{(m+1)} - \Delta^{(m)}}{|F^{(m+1)} - F^{(m)}|}, \quad \delta F^{(m)} = \frac{F^{(m+1)} - F^{(m)}}{|F^{(m+1)} - F^{(m)}|}. \quad (2.41)$$

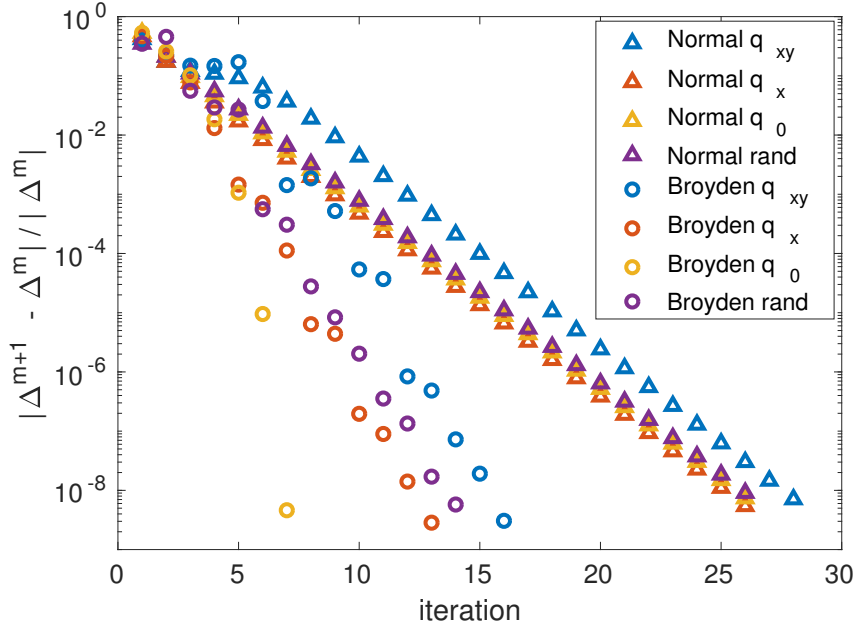


Figure 2.8: The relative error of the order parameter as a function of the iteration for the simple and Broyden self-consistent iteration procedures. The convergence of error is shown for a square lattice with of size 21×21 and parameters $h = 0$, $\mu = 0.8$, and $T = 0.1$, corresponding to a BCS phase. The interaction strength is $U = -3.3t$. The triangles and circles correspond to the simple and Broyden iterations, respectively. The different colors represent different initial ansatz for the order parameter. Every initial ansatz converge to the same uniform BCS state.

To demonstrate the convergence of Δ , a relatively small square lattice, 21×21 sites, is studied with periodic boundary conditions. The temperature is $T = 0.1t$ and the interaction strength is $U = -3t$. The relative error as a function of the iteration is shown in Fig. 2.8 for a parameter range that corresponds to a uniform BCS phase, a phase where $\Delta_i = \Delta_0$. The convergence is shown for four different initial ansatz for both simple and Broyden iterations. For a uniform BCS phase, the initial ansatz has no effect on the converged result. For simple iteration every ansatz converges as fast but the ansatz q_{xy} that has an initial order parameter that oscillates in both x and y directions and is thus the farthest from the correct uniform solution has the largest initial error. The convergence of the Broyden iteration is noticeably faster and the effect of the initial ansatz is larger. There the convergence is affected by how close to the correct solution the initial ansatz is.

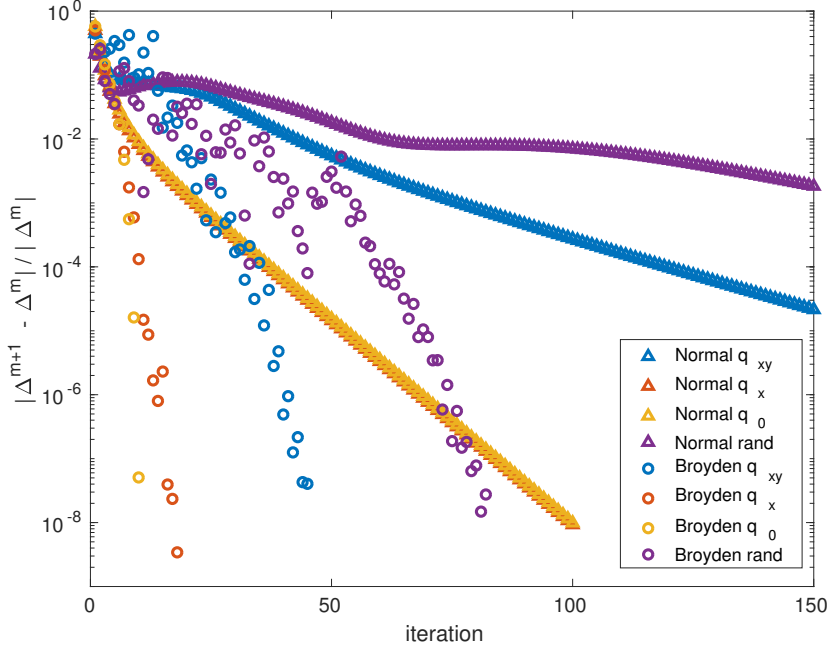


Figure 2.9: The relative error of the order parameter as a function of the iteration for the simple and Broyden self-consistent iteration procedures. The convergence of error is shown for a square lattice with of size 21×21 and parameters $h = 0.55$, $\mu = 0.8$, and $T = 0.1$, corresponding to an LO phase. The interaction strength is $U = -3t$. The triangles and circles correspond to the simple and Broyden iterations, respectively. Different initial ansatz include order parameters oscillating in both x - and y -directions, oscillating in x -direction, being uniform, and random, denoted with q_{xy} , q_x , q_0 , and rand, respectively. The converged phases and free energies for different initial ansatz are shown in Table 2.1.

The convergence of the iterations for a phase where the order parameter is oscillating, an LO phase, is shown in Fig.2.9. Compared to the previous BCS phase, the LO phase is more sensitive to the initial ansatz. Here, the initial ansatz has to be close to the optimal solution to obtain the solution with minimal energy. The converged solutions from different initial ansatz together with the corresponding grand canonical energies are shown in Table 2.1. For the Broyden iteration, the initial ansatz has a small effect on the convergence of error. For the simple iteration however, the initial ansatz seems to have a larger effect. Based on these results, Broyden iteration process is a clear choice over the simple iterations. If the Broyden iteration converges, it is faster than the simple iteration. However in practice, Broyden iterations were often found to not converge at all. In this thesis simple

Table 2.1: The final phases and energies for converged iterations with different initial ansatz of the order parameter for the parameters of Fig. 2.9. The grand canonical energies Ω are calculated with Eq. (2.36).

	Initial ansatz	Ω	converged phase
Simple	LO $q_x + q_y$	-0.291	LO $q_x + q_y$
	LO q_x	-0.169	BCS
	uniform	-0.169	BCS
	random	-0.282	LO q_x
Broyden	LO $q_x + q_y$	-0.291	LO $q_x + q_y$
	LO q_x	-0.169	BCS
	uniform	-0.169	BCS
	random	-0.216	BCS

iterations are used for their stability and predictability.

An important practical aspect to keep in mind when using the components of an eigenvector, is that numerical diagonalisation procedures return eigenvectors with a random phase. Because, if $|n\rangle$ is an eigenvector of a matrix H , then $e^{i\theta}|n\rangle$ is as well. The eigenvectors of a real symmetric matrix can be chosen to be real, but they can still be multiplied by ± 1 and remain as eigenvectors. In the derived result for the order parameter Eq. (2.24), the matrix elements are always multiplied by elements from the same eigenvector, which negates the problem of the random sign from the numerical diagonalisation.

Chapter 3

Results

In this thesis, the Bogoliubov de Gennes equations (BdG) are solved iteratively in real space. BdG Hamiltonian is used to study spin-imbalanced superfluidity in reciprocal space, typically by minimizing the grand canonical energy [46–49]. BdG equations are also employed in real space calculations [39, 40]. In reciprocal space, the lattice periodicity is used to decrease the degrees of freedom, but in real space the number of atoms or lattice sites makes the minimization of the energy unpractical. That leaves the iterative solving of the BdG equations as the most viable option. This section begins with the comparison of the obtained real space superconductivity phase diagram to the one presented in [46, 47] obtained in reciprocal space. Subsequently, the effects of the open boundary conditions are studied. After confirming that the used method is able to reproduce earlier results, the point of interest moves on to quasicrystals. The first studied quasicrystal is the one dimensional Fibonacci chain. After the simple 1D model, the focus moves towards two dimensions. Studies in 2D begin by breaking the lattice periodicity of a square lattice to form a Fibonacci lattice. Finally, the superconducting phases are studied in a true 2D quasicrystal formed from the Ammann-Beenker tiling.

Square lattice

The superconducting phase diagram for the effective magnetisatic field h as a function of the average chemical potential μ is investigated for a square lattice with periodic boundary conditions. The same phase diagram is presented in [46], where it was obtained through the minimization of the grand potential with respect to the order parameter amplitude Δ and the FF wavevector \mathbf{q} . This gives the opportunity to confirm the implementation of the iterative

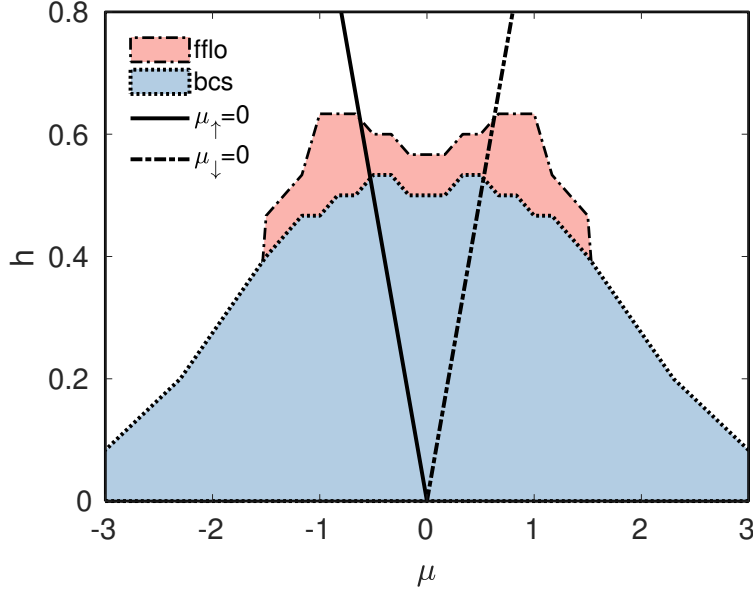


Figure 3.1: Phase diagram for a square lattice of size 27×27 for h over μ at $T = 0.1$ with periodic boundary conditions. The interaction strength $U = -3t$. The solid and the dashed lines show where the chemical potentials of the up and down components are at the highest density of states, respectively.

approach.

The phase diagram for the square lattice is investigated for interaction strength $U = -3t$ and temperature $T = 0.1t$. The temperature is chosen from the range where an oscillating FFLO phase should exist. The interaction and temperature are given in the units of the tunneling strength t . The phase diagram is calculated for the effective magnetic field $h = (\mu_{\uparrow} - \mu_{\downarrow})/2$ as a function of the average chemical potential $\mu = (\mu_{\uparrow} + \mu_{\downarrow})/2$. For a given h , the chemical potential for the up component is $\mu_{\uparrow} = \mu + h$ and for the down component $\mu_{\downarrow} = \mu - h$. The simulated lattice contains $27 \times 27 = 729$ lattice sites with periodic boundary conditions. The diagram is shown in Fig. 3.1.

For small values of h , the obtained superconducting phase is a BCS phase. In the BCS phase the order parameter Δ is uniform and the spin components have the same filling, resulting in an unpolarized phase. When h is increased the system will experience a phase transition to a phase where the order parameter Δ_i oscillates. This oscillating order parameter in real space will be denoted as the LO phase, where $\Delta_i = \Delta_0 \cos(\mathbf{q} \cdot \mathbf{r})$. The LO phase is found at high values of h when the chemical potential difference of the spin components is large, between BCS and normal phase. When h is increased further the system goes into the normal state, because energy difference between the

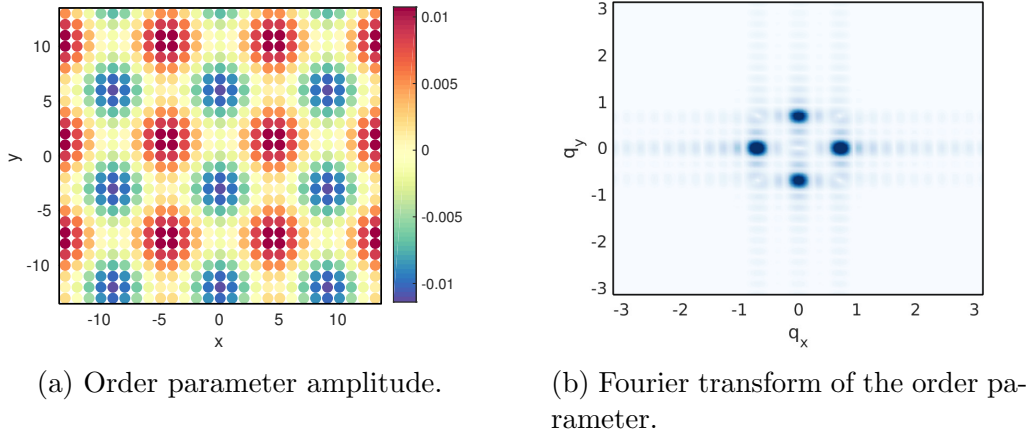


Figure 3.2: a) The order parameter amplitude Δ_i for a square lattice of size 27×27 with periodic boundary conditions. The interaction strength is $U = -3t$ and the temperature is $T = 0.1t$. When the effective magnetic field h is large, the state with the lowest energy is a non-uniform LO phase. This state is obtained with parameters $h = 0.57$ and $\mu = 0$. b) The Fourier transform of Δ_i . The nonzero maximum Fourier component also shows the oscillation of the order parameter.

spin components is too large for pairing to occur. The superconducting phases reach largest values of h close the half filling, where the square lattice density of states is the highest. The LO phase is enhanced when one of the spin components is at the half filling at $\mu_\sigma = 0$, shown as black lines in Fig. 3.1. When moving towards higher h inside the LO phase, the order parameter amplitude keeps decreasing and amplitude of the wavevector \mathbf{q} increases, resulting in higher frequency oscillations.

The typical explanation for the oscillating phase is the nesting of the Fermi surfaces, shown in Fig. 2.7. However, in the real space approach, examination of the momentum space is difficult and information about the nesting is lost. This also requires indirect means to determine whether the system is in the BCS phase or the LO phase. Here the final order parameter is Fourier transformed. For the BCS state the maximum Fourier component is found at zero frequency, corresponding to uniform order parameter. In an LO state the rotational symmetry of the order parameter is broken and the maximum component of the Fourier transformation is found at a nonzero frequency value. This method of determining the phase is accurate for almost uniform lattices but is later found to be inadequate for quasicrystals. Typical order parameter amplitude for the LO phase and its Fourier transform are shown in Fig. 3.2.

Here, the phase diagram is obtained through a self-consistent iterative

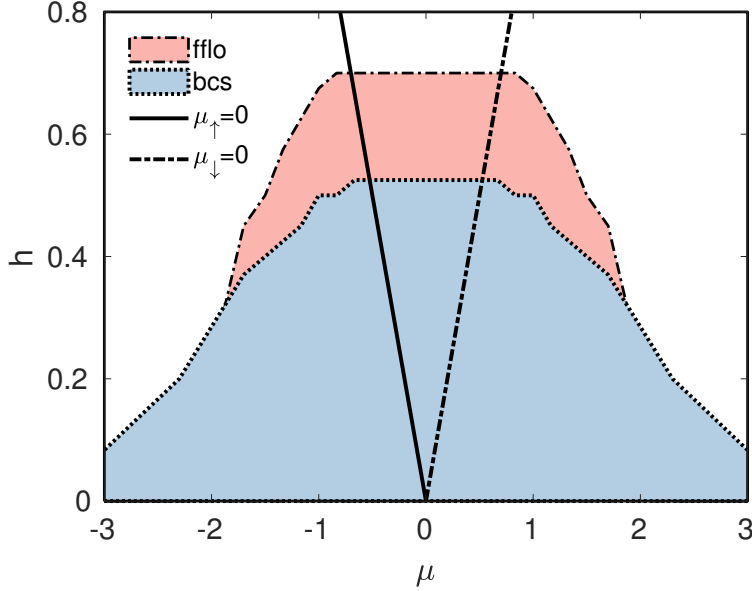


Figure 3.3: Phase diagram for a square lattice of size 27×27 for h over μ at $T = 0.1$ with open boundary conditions. The interaction strength $U = -3t$. The solid and the dashed lines show when the chemical potentials of the up and down components are at the highest density of states, respectively.

approach. In the iterative approach, order parameter is given an initial guess and as a result of the iterations, order parameter amplitudes at each site are obtained. In the iterative approach, the initial ansatz plays a significant role. For a square lattice, an initial uniform ansatz might converge into a normal state where $\Delta = 0$ instead of the energetically favourable state with finite non-uniform order parameter. This requires letting the iterations to converge for both an uniform and an oscillating ansatz and taking the converged result with the lower free energy. To obtain the LO phase, an actually oscillating initial ansatz is not a requirement, but the ansatz should have some non-uniform component. A random ansatz is also possible but it was found that random ansatz has difficulty on converging to a single phase or a single oscillating frequency within LO phase. Random ansatz inside the BCS phase results in a uniform BCS phase.

The obtained phase diagram shows very good agreement with the reference diagram in Ref. [46, 47], where the phase diagram is given for interaction strength $U = -3.3t$. This gives confidence that the iterative approach can be used to accurately predict the possible superconducting phases. It was noted that inside the LO phase, the amplitude of the wave vector of \mathbf{q} increases with increasing h , consistent with Ref. [49].

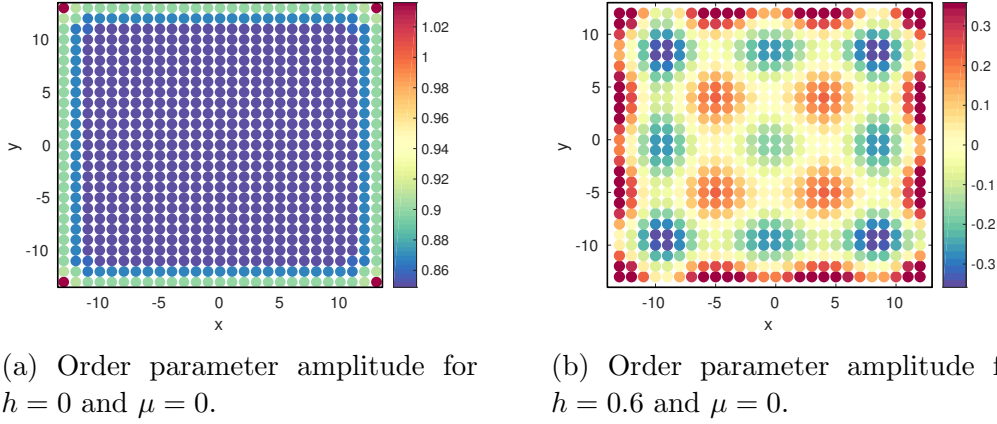


Figure 3.4: The order parameter amplitudes Δ_i for a square lattice of size 27×27 with open boundary conditions for a) BCS phase and b) LO phase. The interaction strength is $U = -3t$ and temperature is $T = 0.1t$. The order parameter amplitude is larger at the boundaries of the system. The behaviour of Δ_i close to the centre of the lattice is similar to the behaviour in the lattice with periodic boundaries.

Effects of the open boundary conditions

Simulating lattice structures with periodic boundary conditions (PBC) only allows to investigate the behaviour of approximant quasicrystals, which are lattices with large unit cells. The purpose of this section is to see how open boundary conditions (OBC) affect the phase diagram and the obtained superconducting states. Since a true quasicrystal has no periodicity at all, it is important to study whether the effects of the open boundary conditions can dominate the effects of the quasicrystal lattice structure.

The superconducting phase diagram for effective magnetic field h over the average chemical potential is shown in Fig. 3.3 for open boundary conditions. The interaction strength is $U = -3t$ and temperature is $T = 0.1t$, the same as for the previous system with PBC. The largest difference to the PBC phase diagram can be seen at half filling at $\mu = 0$. There the superconducting phases extend to higher h than for PBC. The parameter range of the LO phase has also increased. This increase can in part be understood as consequence of the reduction the dimensions of the system. The boundaries of the system are not completely 2D systems and in systems with lower dimensions, the amplitude of the order parameter can increase.

The typical order parameter amplitudes for a BCS phase with OBC are shown in Fig. 3.4a, where the effects of the open boundaries is clearly visible. The order parameter amplitude is increased at the boundaries of the system

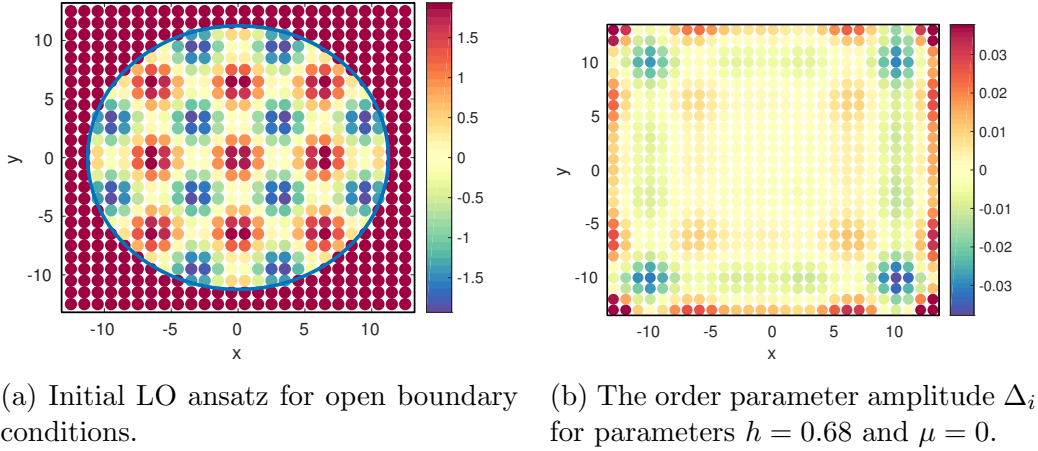


Figure 3.5: b) Δ_i for a square lattice of size 27×27 with open boundary conditions. Temperature is $T = 0.1t$ and the interaction strength is $U = -3t$. For these parameters, the state with the lowest energy with periodic boundary conditions was a normal phase, instead of the found LO phase with the open boundary conditions.

and is highest at the corners of the lattice. Close to the center of the lattice the order parameter amplitude is almost uniform.

The typical order parameter amplitudes for the oscillating LO phase are shown in Fig. 3.4b. Also here, the order parameter amplitude is larger at the boundaries of the system. The oscillation frequency and phase are changed by the boundaries to reflect the size and the shape of the lattice. This suggests that the stability of the LO phase found in lattice with OBC depends on the lattice size. The oscillations take the form of standing waves inside the lattice. With OBC the oscillations reach the boundary of the grid and break the uniformity of the edge sites.

The obtained LO phase with OBC is greatly affected by the initial ansatz and with a simple oscillating initial Δ , the system fails to converge to a state with a single oscillating mode. Instead, for a simple ansatz, the order parameter often has modes oscillating in different directions in different parts of the lattice. The final order parameter with only a single oscillating mode typically had the lowest energy. An initial ansatz that allows the system to converge into a single oscillating mode is shown in Fig. 3.5a. In this ansatz, the oscillations start in the middle and then propagate towards the boundaries with iterations.

The extension of the LO phase boundary towards higher h might not be stable in the thermodynamic limit. The order parameters at a parameter range that corresponded to a normal state with PBC are shown in Fig. 3.5b. For these parameters, the amplitude of the oscillations goes to zero

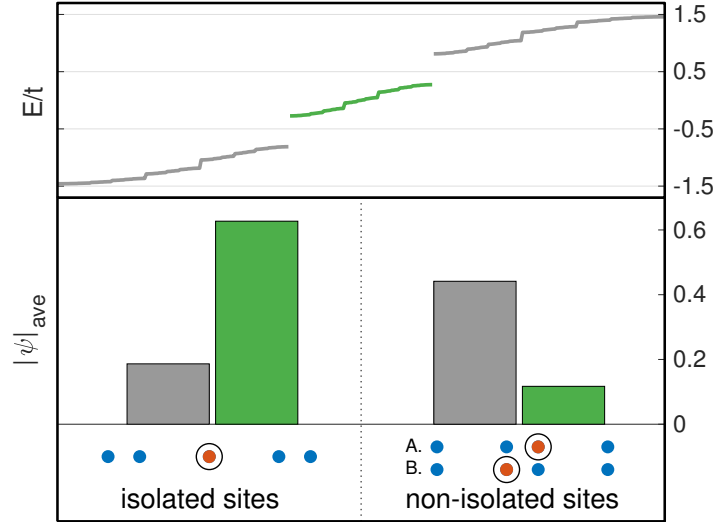


Figure 3.6: The amplitudes of the non-interacting eigenvectors at the three different possible site configurations of the Fibonacci chain with length $L = 377$. The top panel shows the non-interacting energy spectrum. The middle panel shows the average amplitude of eigenvectors on the bottom and the middle bands, marked with grey and green, respectively. The left side of the middle panel shows the average amplitude at the isolated sites and the right panel shows the average amplitude at sites that are connected to neighbouring sites by one long interval.

at the center of the lattice. This behaviour might dominate over the effects caused by the aperiodicity. To combat these extra difficulties, the superconducting phases in quasicrystals will be studied only with periodic boundary conditions.

Pairing in Fibonacci chain

The effect of breaking the translational symmetry is studied first in the 1D Fibonacci chain. The local fluctuations of the system increase as the dimension of the system is reduced and hence, the mean-field predictions in one-dimension must be interpreted cautiously. The 1D case is used to gain understanding on the possible origins of different superfluid phases in quasicrystals. The knowledge of the different phases in 1D can also be used to engineer better initial ansatz for 2D systems. The effects of breaking the translational symmetry on the convergence of the iterations with different

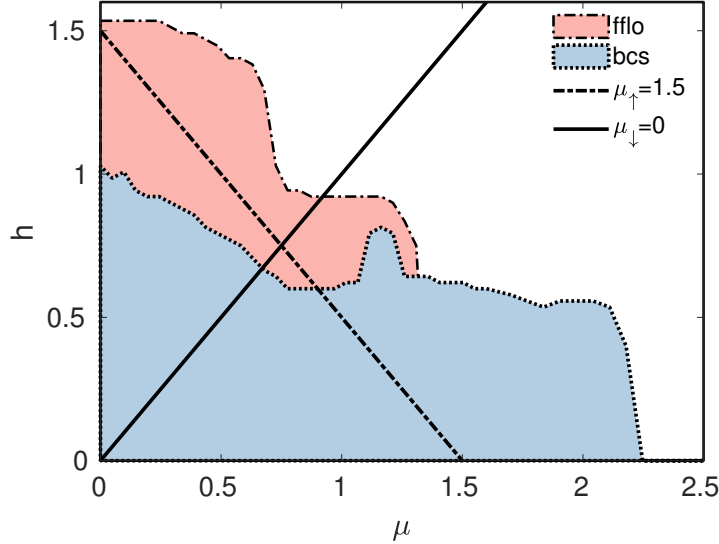


Figure 3.7: Phase diagram based on the maximum component of the Fourier transformed order parameter Δ_i . This Fibonacci chain has a length of $L = 377$ and long hopping $t_l = 0.53$. When the largest amplitude Fourier component of Δ_i is nonzero, the state is considered to be an LO state. The interaction strength is $U = -3t$ and temperature is $T = 0.1t$.

ansatz are also easier to understand in 1D.

When moving from a chain of uniformly coupled lattice sites to a Fibonacci chain, the continuous energy band of the noninteracting particles splits into three main energy bands, which are further divided into smaller subbands. The free particle eigenenergies can be divided into three main bands. The energy bands corresponding to the lowest and highest energies are symmetric around $E = 0$. The behaviour of the eigenvector of these bottom and top bands differ qualitatively from the behaviour of the eigenvectors of the middle band. In the middle energy band, the eigenvectors are focused on the isolated sites of the chain whereas on the top and bottom bands, the eigenvectors are focused on the non-isolated sites. Here, a site is called isolated if it is connected to both of its neighbours with a long interval. The behaviour of the eigenvectors and the three possible site configurations are visualized in Fig. 3.6. The behaviour of the non-interacting Fibonacci chain will be important for understanding the phase diagram of the interacting system.

The Fibonacci chain considered here has a length of $L = 377$. The length of the chain is chosen as a Fibonacci number because this makes the height field zero at the both ends of the chain (see Fig. 2.3a). In this section

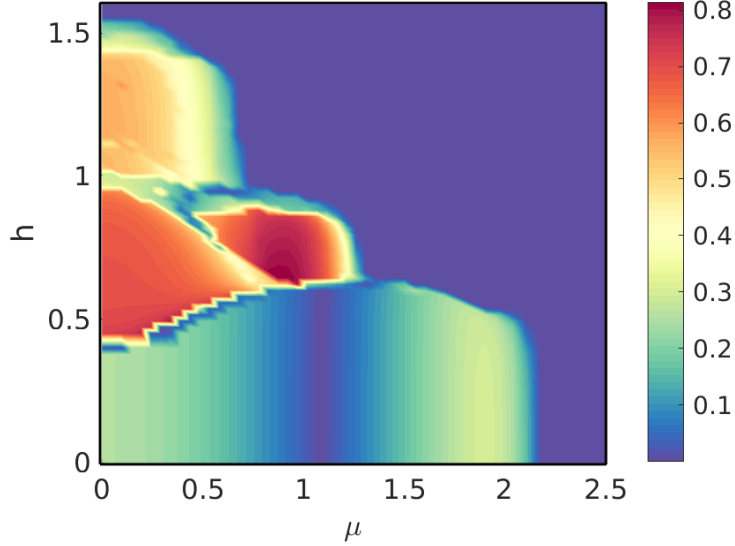


Figure 3.8: The absolute value of the difference of the order parameters averaged over the isolated sites and the non-isolated sites. Parameters are the same as in Fig 3.7. Four distinct regions can be seen in the figure, a region with an almost uniform BCS phase at small h , two regions with large difference in Δ_i between isolated and non-isolated sites at medium h , and an oscillating LO phase at large h .

the focus is on finite temperature systems with attractive on-site interaction between the particles. The phase diagrams presented here are calculated for a system with temperature $T = 0.1t$ and interaction strength $U = -3t$. Different pairings in the chain are investigated as a function of the average chemical potential $\mu = (\mu_\downarrow + \mu_\uparrow)/2$ and the effective magnetic field $h = (\mu_\uparrow - \mu_\downarrow)/2$.

In the 2D square lattice, an LO state is found with increasing h . In the LO state the order parameter oscillates as $\Delta_i = \Delta_i \cos(\mathbf{q} \cdot \mathbf{r}_i)$ (LO state) or as $\Delta_i = \Delta_i e^{i\mathbf{q} \cdot \mathbf{r}_i}$ (FF state). Similar to the initial phase diagram with 2D square lattice, the first step is to categorize the different configurations of the order parameter through a Fourier transformation. With this approach a state is denoted as an LO state when the maximum Fourier component has nonzero frequency. The phase diagram based on the Fourier transformations is presented in Fig. 3.7. Here a phase with an oscillating Δ is found to exist on top of the BCS phase. The black line on the phase diagram shows when the chemical potential of the up component is at the rightmost peak of the noninteracting DOS, shown in Fig. 2.4. The high density of states seems to enhance an oscillating phase. This is in good agreement with previous results on different lattices [46, 48].

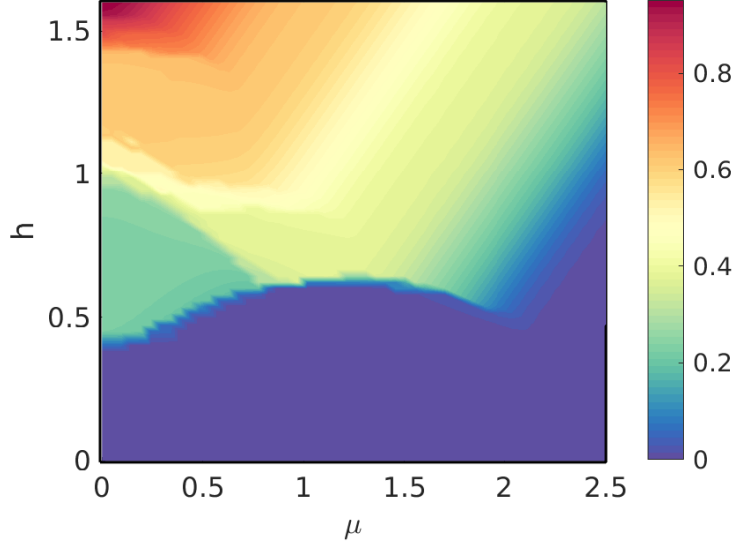


Figure 3.9: The polarization in the Fibonacci chain, calculated as the average of $n_{i\uparrow} - n_{i\downarrow}$. Parameters are the same as in Fig 3.7. A typical unpolarized BCS phase can be found at small h . Above this phase, at small μ , is a polarized phase with clear boundaries. The two oscillating phases at large h do not have as sharp boundaries as the BCS phases.

However, a simple distinction between a uniform BCS state and an oscillating LO state is not as clear for the Fibonacci chain. The aperiodic chain results in complex orderings of the order parameters. To visualise the regions of the phase diagram with different behaviours, the difference between the order parameters averaged over the isolated sites and the non-isolated sites is shown in Fig. 3.8. The average polarizations of different regions are also shown in Fig. 3.9. These figures show how even the BCS state is non-uniform and in fact the actual phase diagram could consist of at least four different regions. The lower part of the phase diagram corresponds to an almost BCS phase where the polarization is zero and the order parameter is close to uniform. At low values of μ , but towards larger h above the first phase, exists a second phase with finite polarization. Inside this phase the order parameter amplitude experiences a large decrease at the isolated sites. The third phase is found above the BCS phase and to higher values of μ from the polarized BCS phase. This phase is similar to the second phase, but the amplitude of the order parameter is small in the non-isolated sites and large at the isolated sites. This region also hosts a larger polarization than the second phase. An LO type phase is found to exist on top of these BCS type phases. The oscillations of the order parameter do not strictly follow any sinusoidal function but seem to show characteristics of the aperiodic lattice structure.

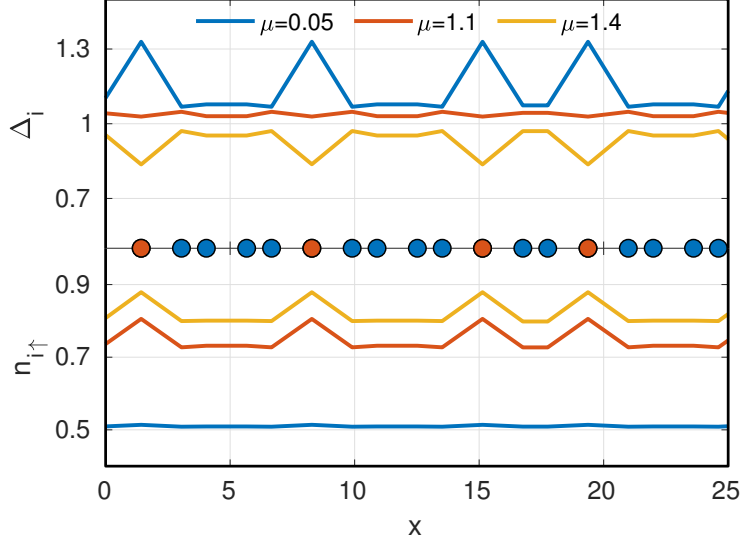
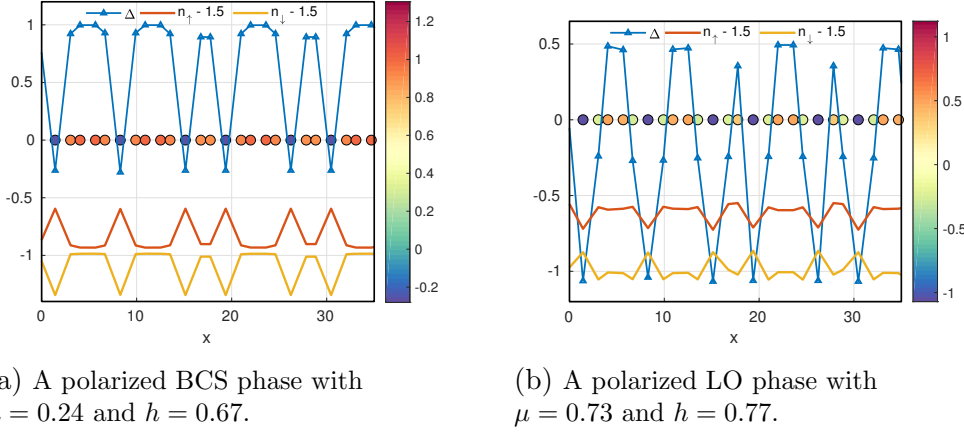


Figure 3.10: The order parameter amplitude Δ and the densities $n_{i\uparrow}(=n_{i\downarrow})$ on a section of a Fibonacci chain with $L = 377$. Data is shown for $h = 0.21$ and three different μ , corresponding to the typical BCS phase. The lattice sites are shown in the middle for visualisation.

In the phasediagram based on the Fourier components, the third phase was denoted as an LO type phase, but is in reality closer to the second BCS type phase.

The observed four phases are then examined closer. The first studied phase is the non-polarized BCS type phase that is found for small h . There both spin components occupy the same energy band. The behaviour of Δ_i in the BCS type phase is shown in Fig. 3.10 for parameters $h = 0.21$ and three different $\mu = \{0.05, 1.1, 1.4\}$. Initially at $\mu = 0.05$, Δ_i is higher at the isolated sites. In the non-interacting energy spectrum both components occupy states in the middle energy band, a band that is focused on the isolated sites. Moving towards higher μ but staying inside the BCS region, the order parameter amplitude at the isolated sites begins to decrease. For $\mu = 1.1$, Δ_i is almost uniform over the entire lattice. For $\mu = 1.4$, Δ_i is smaller at the isolated sites than in the non-isolated sites. This can be understood through the non-interacting eigenstates. As μ is increased, both components move towards the higher energy band that is focused on the non-isolated sites. This decreases the pairing at the isolated sites. The behaviour of Δ_i changes when moving towards the higher energy bands but the densities n_i are always larger at the isolated sites.



(a) A polarized BCS phase with $\mu = 0.24$ and $h = 0.67$.

(b) A polarized LO phase with $\mu = 0.73$ and $h = 0.77$.

Figure 3.11: The order parameter amplitudes Δ and the densities of different components on a section of a Fibonacci chain with $L = 377$ sites. The order parameter amplitude Δ_i is equal at every site with identical nearest neighbour configuration.

Increasing the effective magnetisation to $h = 0.67$, order parameter Δ_i at the isolated sites becomes negative. This phase, shown in Fig. 3.11a, is still considered a BCS phase. But the finite polarization of this phase is a distinct difference from the typical BCS. On the isolated sites, the density of the up-components is increased and density of the down components is decreased. For small μ one of the spin components still lies on the middle energy band. When h is increased the other component moves to the top or bottom energy band. This phase emerges as the two different type eigenvectors interact. The convergence of the iterative method to this phase requires a specialized ansatz where initial order parameter is set to small negative values at the isolated sites. This ansatz follows the local lattice geometry and it was found by calculating the energies of different final states (see Fig. A.1).

Staying close to the $h = 0.7$ and moving towards larger μ brings the systems into a third phase. The behaviour of Δ_i in this phase is shown in Fig. 3.11b. In this phase the maximum Fourier component is found at a nonzero frequency and the phase is denoted as an LO phase. Compared to the polarized BCS phase, the polarization is increased further but is now smaller at the isolated sites. The largest difference to the polarized BCS phase is that Δ_i at sites next to the isolated sites have decreased in amplitude and the maximum amplitude of the order parameter is now found at the isolated sites. This phase still follows the local lattice configuration and is thus called the lattice LO phase.

The final fourth phase can be found at the highest values of h . This phase is denoted as an LO phase. The behaviour of the order parameter is shown

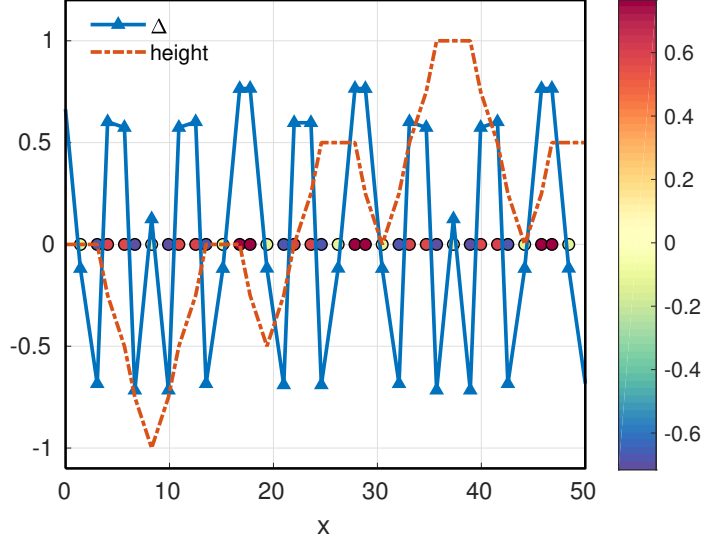


Figure 3.12: The order parameter amplitudes Δ_i on a section of the Fibonacci chain with $L = 377$ sites for $h = 1.05$ and $\mu = 0$, corresponding to an LO phase. The height field is shown together with Δ_i (see Fig. 2.3a). This is a demonstration of an oscillating phase where Δ_i is not equal at sites with identical nearest neighbour configuration.

in Fig. 3.12 for $h = 1.05$. This phase is different from the previous lattice LO phase because it does not follow the local lattice configuration; the order parameter amplitudes are no longer the same at similar sites. The oscillations however seem to follow a longer range order. The order parameters are the same for sites that correspond to maxima or minima in the height field, e.g. for $x \approx 9$ and $x \approx 37$. The height field can be thought as a measure of similarity of sites that considers more than just the nearest neighbour configurations. Between these two different LO phases is an area of phase separation. There the polarization changes linearly from the polarization of the lattice LO phase to the polarization of the lattice breaking LO phase. The oscillations in this phase show complex patterns that rise as a superposition of the two oscillations.

Fibonacci lattice

A simple two-dimensional analogue of the Fibonacci chain can be obtained by modifying the tunneling amplitudes in a square lattice according to the Fibonacci chain. This could be thought as stacking of Fibonacci chains in two different directions. The temperature is $T = 0.1t$ and the interaction

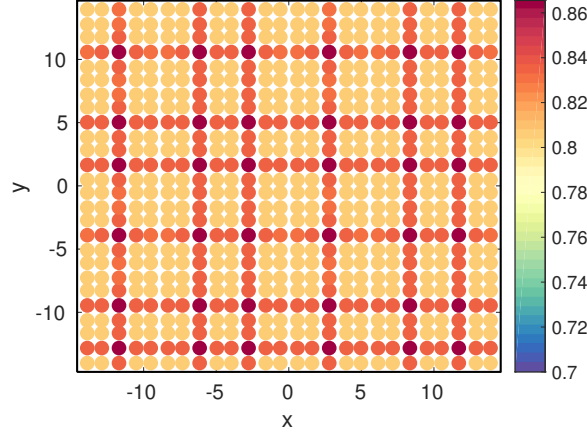
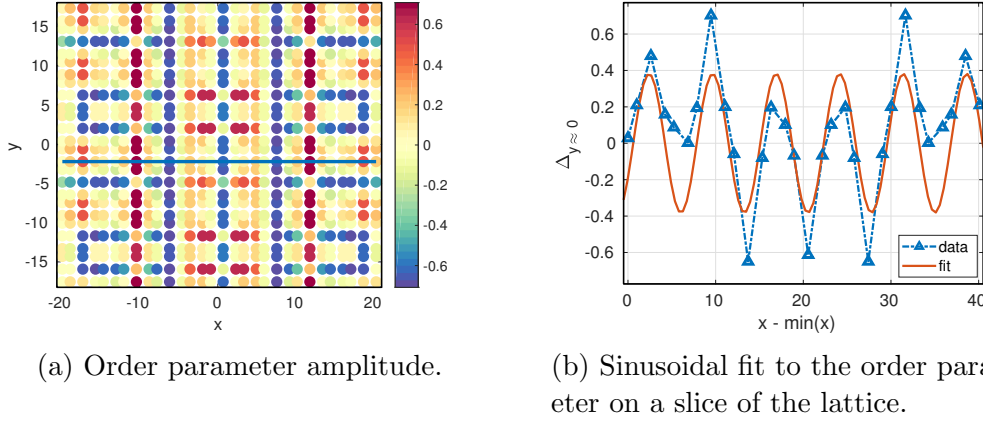


Figure 3.13: The order parameter amplitude Δ_i for a Fibonacci lattice of size 27×27 with periodic boundary conditions. This is a demonstration of a state without spin-imbalance, with parameters $h = 0$ and $\mu = 0.83$. The parameter $a = 0.3$ results in a long hopping amplitude $t_l = 0.83t_s$. Temperature is $T = 0.1t$ and the interaction strength is $U = -3t$.

strength is $U = -3t$. The parameter a that changes the distance of the long intervals in the chain is set to $a = 1$, giving tunneling amplitudes $t_l = 0.53$. Tunneling amplitudes for the short intervals are $t_s = 1$. The DOS of the two-dimensional Fibonacci lattice is significantly different from the DOS of the Fibonacci chain. For the Fibonacci chain the DOS shows energy gaps already for small values of a . For the Fibonacci lattice, gaps appear only after $a > 2$, which corresponds to tunneling amplitudes $t_l \approx 0.13$. Here, the parameter $a = 1$ results in a gapless DOS.

An example of the Δ_i in the Fibonacci lattice for a BCS phase are shown in Fig. 3.13. Compared to the 1D Fibonacci chain where sites could be divided into isolated and non-isolated sites, in 2D lattice there also exist sites that are isolated in both x and y directions, denoted as doubly-isolated sites (DIS). The order parameter amplitude is higher on the sites that are less connected to the neighboring sites, and highest on the DIS. The order parameter amplitude is equal on every site with the same nearest-neighbor configuration.

The phase diagram of the Fibonacci lattice is similar to the square lattice. However, the oscillating LO phase is vastly different from the same phase in the square lattice. The order parameter Δ_i for the oscillating phase is shown in Fig. 3.14a. Instead of an order parameter that oscillates sinusoidally $\Delta_i \approx \cos(\mathbf{q} \cdot \mathbf{r})$, the order parameter seems to have obtained aperiodic components. A sinusoidal fit to the Δ_i at $y \approx 0$ is shown in Fig. 3.14b.



(a) Order parameter amplitude.

(b) Sinusoidal fit to the order parameter on a slice of the lattice.

Figure 3.14: a) The order parameter amplitude Δ_i for a square lattice of size 27×27 with periodic boundary conditions. With parameters $h = 0.58$ and $\mu = 0$, the state with the lowest energy is a non-uniform LO phase. Temperature is $T = 0.1t$ and the interaction strength is $U = -3t$. b) A sinusoidal fit to Δ_i at $y \approx 0$.

Pairing in Ammann-Beenker lattice

True quasicrystals show rotational symmetries that are forbidden for periodic crystals. However, keeping the lattice periodic avoids the large effect of the open boundaries, as seen in Section 3.2. Ammann-Beenker tiling is a space filling tiling that can be made periodic and has eight-fold rotational symmetry, which makes it the closest model of a true quasicrystal considered in this thesis. The eight-fold rotational symmetry originates from the high-symmetry sites that have connections to eight neighboring sites, marked with black circles in Fig. 3.15. The lattice Hamiltonian is constructed from the Ammann-Beenker tiling by considering the nodes of the tiling as the lattice sites. Only the nearest neighbour nodes are considered connected, which leaves the diagonals of the squares unconnected. See Fig. A.5a for all of the connections between nodes with open boundary conditions. It is noted that the underlying tiling has the same configuration of tiles on the opposite sides of the lattice, which allows the formation of a Hamiltonian with periodic boundaries. In a periodic system three new high-symmetry sites are formed at the boundaries of the lattice.

The non-interacting density of states of the Ammann-Beenker tiling, shown in Fig. A.5b, has a sharp peak at half filling, similar to the square lattice. Here the behaviour of the order parameter is examined for Ammann-Beenker tiling with three inflations, resulting in 264 sites. Interaction strength between different spin components is $U = -3t$ and the temperature is

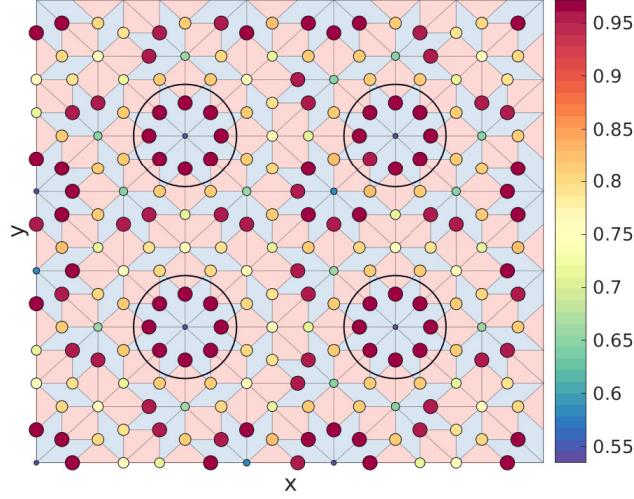


Figure 3.15: The order parameter amplitudes for Ammann-Beenker tiling inflated three times with $N = 264$ nodes. The size of the circle is proportional to the amplitude of the order parameter. The parameters $h = 0$ and $\mu = 0$ correspond to a BCS phase. The tiling is drawn as a visual guide and the black circles mark the high-symmetry sites.

$T = 0.1t$. The tunneling amplitudes between the connected sites are set to $t = 1$.

A demonstration of a typical BCS phase in Ammann-Beenker lattice is shown in Fig. 3.15. In the figure, the four high-symmetry sites in the center are circled. For three inflations, these high-symmetry sites are ordered symmetrically. Although harder to notice, a fifth high-symmetry site is located at the corner site of the lattice and the sixth and the seventh high-symmetry sites are at the borders of the lattice. The order parameter amplitude in this tiling behaves strictly according to the underlying lattice geometry. The order parameter amplitude is equal at every site with the same closest neighbour configuration. The sites with the highest number of connections, the high-symmetry sites, have the smallest order parameter amplitude. The sites with the lowest number of connections, neighbors of the high-symmetry sites, have the highest order parameter amplitude. This phase is labelled as a BCS state due to the dominating zero-frequency component of the Fourier transform of the order parameter amplitude, shown in Fig. 3.16. The second highest peaks in the first Brillouin zone show the eight-fold rotational symmetry of the lattice. The four large amplitude peaks at the corners are the four of the next eight peaks visible. The eightfold rotational symmetry of the lattice is thus preserved in the order parameter amplitude, marking a clear

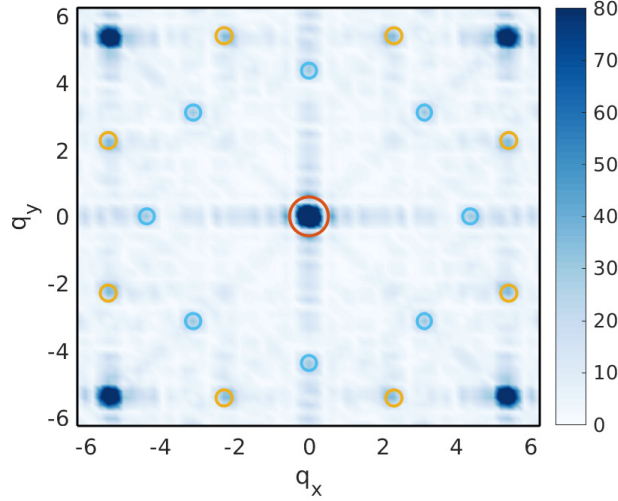


Figure 3.16: The Fourier transformation of Δ_i , shown in Fig. 3.15, for Ammann-Beenker tiling with $N = 264$ nodes and a BCS state without spin-imbalance $h = 0$. The circles denote peaks in the Fourier spectrum and the radius of the circle is proportional to the height of the peak. The yellow peaks have slightly larger amplitude than the light blue peaks. Only peaks with $|q| < 2\pi$ are marked.

difference to any periodic lattice.

The LO phase in Ammann-Beenker lattice

In the Fibonacci chain, at a high spin-imbalance h , an oscillating phase broke the symmetry of the similar sites. The oscillating phase in the Fibonacci chain was not random, and seemed to follow a longer range order described by the height field. This order was not found in the two-dimensional Fibonacci lattice, possibly because this lattice does not show a rotational symmetry forbidden for periodic crystals. However, the Ammann-Beenker tiling seems to support a phase with oscillations that have a longer range order.

The similarity of the DOS of the Ammann-Beenker and the square lattices suggests that an oscillating phase in the Ammann-Beenker lattice could be found in the parameter range that supports an oscillating phase in the square lattice. Indeed, close to the line where $\mu_\downarrow = 0$, Δ_i begins to oscillate as the spin-imbalance h is large enough. Similar to the square lattice, this phase is found at large values h between the BCS and the normal state. The order parameter amplitudes for $h = 0.56$ and $\mu = 0.66$ are shown in Fig. 3.17a. The studied lattice has been inflated 3 times and contains $N = 264$ lattice sites, temperature is $T = 0.1t$, and the interaction strength is $U = -3t$, same

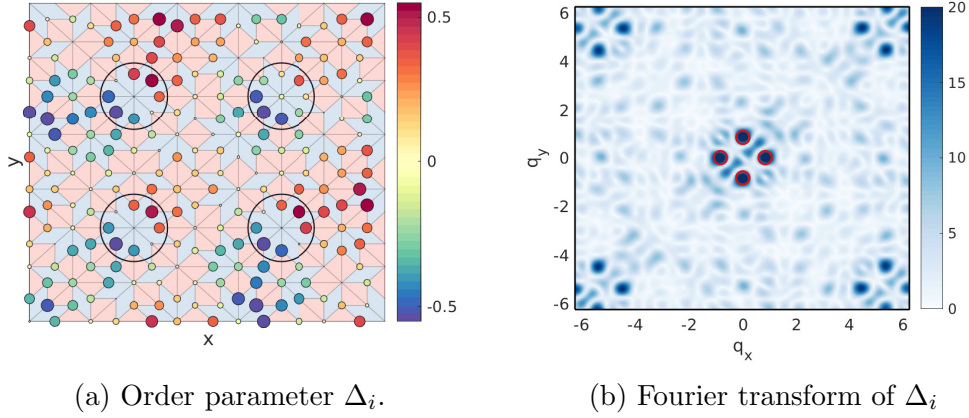


Figure 3.17: Ammann-Beenker tiling with $N = 264$ nodes. The parameters $h = 0.56$ and $\mu = 0.66$ result in an LO state. The tiling is shown as a visual guide. a) The size of the marker denotes the amplitude of the order parameter and the circles denote the high-symmetry sites. b) The Fourier transform of Δ_i . The red circles show the four largest peaks in the transformed components.

as in the previous section.

Inside the BCS-phase, the Δ_i follows the local lattice configuration. In the oscillating phase, Δ_i is no longer equal at the sites with identical nearest neighbour configurations. The oscillations do not completely ignore the underlying lattice geometry, but seem to be focused about the high-symmetry sites, marked with black circles in Fig. 3.17a. With three inflations of the tiling, the high-symmetry sites are ordered symmetrically around the center of the periodic unit cell. This symmetry can be seen in the Fourier transform of the order parameter, shown in Fig. 3.17, where one finds four maximum Fourier components. These four components break the underlying eight-fold lattice symmetry, and would be an example of a phase that ignores the symmetry of the lattice.

To see whether this is a real phase or an artefact of the small unit cell size, the oscillating phase is studied in a larger lattice. The order parameter amplitudes are shown in Fig. 3.18 for the tiling inflated four times, resulting in a lattice with 1452 sites. All the other parameters are kept fixed. The site with the highest symmetry is located at the corners of the four times inflated tiling, and to better visualize the order parameter symmetry, the unit cell is shifted so that the highest symmetry site is at the center. The Fourier transform of this phase, shown in Fig. 3.19, shows a maximum Fourier component at non-zero momentum surrounded by eight circles of local maxima. The Fourier transform of the larger unit cell shows that the oscillating phase follows the lattice symmetry. For the iterative method to

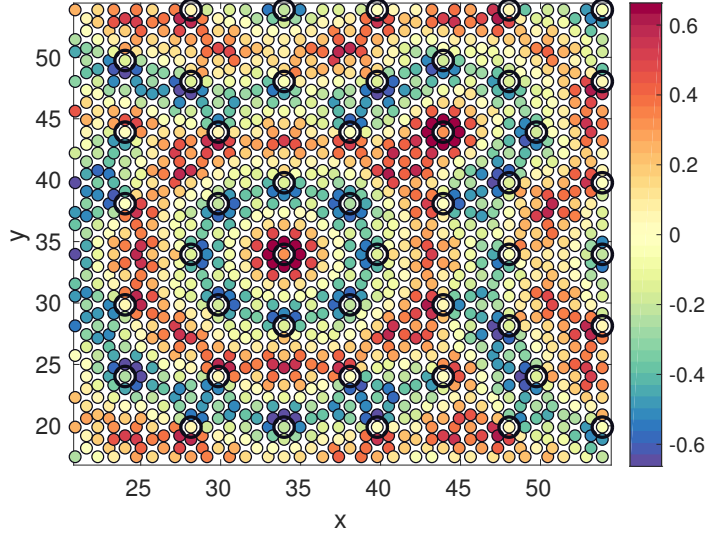


Figure 3.18: The order parameter amplitudes for Ammann-Beenker tiling inflated four times with $N = 1452$ nodes. The parameters $h = 0.56$ and $\mu = 0.66$ correspond to an LO phase, the temperature is $T = 0.1t$, and the interaction strength is $U = -3t$. All of the high-symmetry sites (sites with eight nearest-neighbours) are marked with a black circle.

converge to a phase that follows the lattice symmetry, also the initial ansatz has to follow the lattice symmetry. A lattice symmetry breaking phase, with higher energy, can be found for the larger lattice if the initial ansatz does not follow the lattice symmetry.

In the Fibonacci chain, the oscillations at large h seemed to follow a longer-range lattice order. Similar oscillations that seem random at small length scales but follow some longer range lattice order, are found also in the Ammann-Beenker tiling. To demonstrate this, a patch of a twice inflated tiling is drawn on top of the four times inflated tiling with the high-symmetry sites of the large lattice acting as the nodes of the twice inflated tiling, shown in Fig. 3.20. The order parameter amplitudes at identical sites in this superlattice seem to be the same. However, only few identical sites of the superlattice are visible and it is impossible to say if this holds for a larger lattice. However, it seems that in the Ammann-Beenker tiling, the oscillating LO mode is a phase that does not break the symmetry of similar sites, but rather the equality of sites now refers to the superlattice positions. The oscillating phase in the Ammann-Beenker tiling could thus be called a self-similar LO phase.

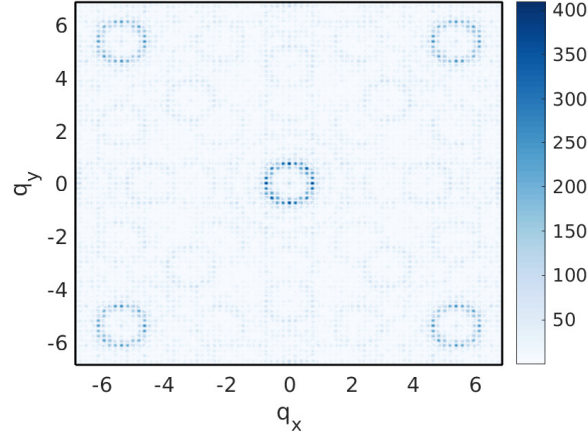


Figure 3.19: The Fourier transform of the order parameter amplitudes shown in Fig. 3.18. A maximum Fourier component has now shifted away from zero frequency. The Fourier component pattern shows eight circles surrounding the center circle, revealing the eight-fold rotational symmetry. The four circles at the corners with large amplitudes belong to the second Brillouin zone.

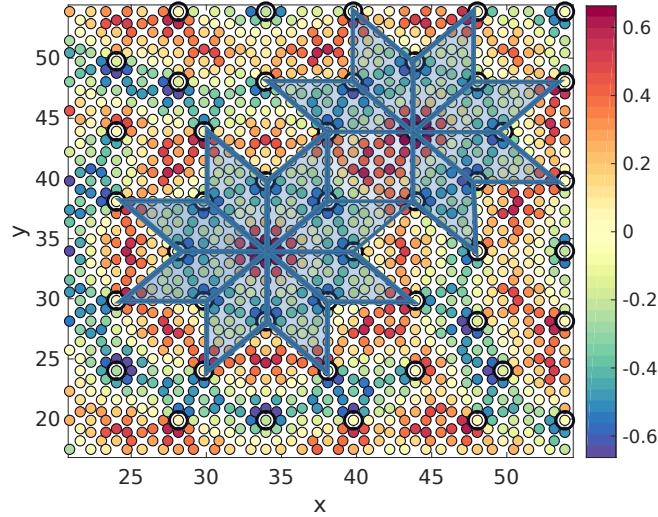


Figure 3.20: The order parameter amplitudes for Ammann-Beenker tiling inflated four times with $N = 1452$ nodes. The parameters $h = 0.56$ and $\mu = 0.66$ correspond to an LO phase, the temperature is $T = 0.1t$, and the interaction strength is $U = -3t$. A twice inflated tiling is drawn on top of the tiling to visualize the self-similar structure of the oscillations. All of the high-symmetry sites have been marked with a black circle. In this figure, the simulated unit cell has been translated to shift the high-symmetry site to the middle. Otherwise it is the same as Fig. 3.18

Chapter 4

Summary

In this thesis, different superconducting phases were studied in quasicrystal analogues, including a one-dimensional Fibonacci chain and a two-dimensional Ammann-Beenker lattice. It was seen that these lattices can host multiple different phases that show characteristics that are not possible for periodic lattices.

The one-dimensional Fibonacci chain was found to host four different superconducting phases. However, the distinction of the different phases to a uniform BCS phase or an oscillating FFLO phase was not possible. The phases were divided into two BCS-type phases and two oscillating phases. The first BCS phase is found at low spin-imbalance and is not polarized whereas the other BCS at larger spin-imbalance is. Both of these phases follow the local lattice geometry. With the increase of the spin-imbalance, the ground state of the system changes into an oscillating phase. The oscillations of the phase with lower spin-imbalance follow the local lattice geometry. Contrary to all previous phases, the phase with the largest spin-imbalance breaks the local lattice geometry. The order parameter amplitudes are found to be the same on sites that have the same long-range environment.

In the Ammann-Beenker lattice a BCS phase is found at a small spin-imbalance. This phase follows the local lattice geometry and thus shows the eight-fold rotational symmetry of the lattice, forbidden for periodic structures. An oscillating phase is found close to the parameter range where it is found in the square lattice. This oscillating phase also follows the underlying lattice symmetry. However, to see this, a large lattice is required. In this oscillating phase, the order parameter amplitudes are no longer the same at the sites with the same nearest neighbour configuration, but at sites that are in a similar position in a less inflated superlattice.

In both the Fibonacci chain and the Ammann-Beenker tiling, the BCS order parameter follows the local lattice symmetry when the spin-imbalance

is small, even though this local lattice configuration is repeated aperiodically. The BCS order parameter is equal at the sites with the same nearest-neighbour configuration. When the spin-imbalance of the components increases an oscillating phase becomes more favorable. In a periodic square lattice every site is equal, which means that an oscillating order parameter breaks this equality of sites. Similarly, even though the oscillating phase does not appear as a clear sinusoidal in a quasicrystal, it marks a phase where the order parameter breaks the similarity of sites with identical nearest neighbor configuration.

It is found that the effect of the initial ansatz on the final state increases when the system is no longer periodic. The final converged phases with order parameters that follow the lattice symmetry were found to be energetically favourable. Especially close to a phase boundary the self-consistent iteration easily converges to a state with larger energy. The accuracy of the mean field theory in one dimension can be questioned and confirmation for the existence of the found phases requires further study with more advanced methods such as density matrix renormalization group (DMRG). With the iterative approach it is also hard to say whether the found states are actually the ground states of the system.

This thesis offers a brief glimpse to the vast world of physics that quasicrystals can offer. Future studies would include the use of more advanced methods to confirm the existence of the found phases. The electronic properties and superconductivity in quasicrystals has not yet been studied in great detail and provide a wide range of possibilities for further studies.

Bibliography

- [1] H. K. Onnes, “The superconductivity of mercury,” *Comm. Phys. Lab. Univ. Leiden*, vol. 122, no. 124, p. 34, 1911.
- [2] J. Bardeen, L. N. Cooper, and J. R. Schrieffer, “Theory of superconductivity,” *Physical Review*, vol. 108, no. 5, p. 1175, 1957.
- [3] D. Shechtman, I. Blech, D. Gratias, and J. W. Cahn, “Metallic phase with long-range orientational order and no translational symmetry,” *Physical Review Letters*, vol. 53, no. 20, p. 1951, 1984.
- [4] D. Shechtman, “The Nobel Prize in Chemistry 2011.” http://www.nobelprize.org/nobel_prizes/chemistry/laureates/2011, 2011. Accessed: 2018-08-09.
- [5] T. Ishimasa, H.-U. Nissen, and Y. Fukano, “New ordered state between crystalline and amorphous in Ni-Cr particles,” *Physical Review Letters*, vol. 55, no. 5, p. 511, 1985.
- [6] L. Chen and F. Spaepen, “Calorimetric evidence for the micro-quasicrystalline structure of ‘amorphous’ Al transition metal alloys,” *Nature*, vol. 336, no. 6197, p. 366, 1988.
- [7] A. Goldman and R. Kelton, “Quasicrystals and crystalline approximants,” *Reviews of Modern Physics*, vol. 65, no. 1, p. 213, 1993.
- [8] A. Schilling, M. Cantoni, J. Guo, and H. Ott, “Superconductivity above 130 K in the Hg–Ba–Ca–Cu–O system,” *Nature*, vol. 363, no. 6424, pp. 56–58, 1993.
- [9] C. Tsuei and J. Kirtley, “Pairing symmetry in cuprate superconductors,” *Reviews of Modern Physics*, vol. 72, no. 4, p. 969, 2000.
- [10] Y. Cao, V. Fatemi, S. Fang, K. Watanabe, T. Taniguchi, E. Kaxiras, and P. Jarillo-Herrero, “Unconventional superconductivity in magic-angle graphene superlattices,” *Nature*, vol. 556, no. 7699, p. 43, 2018.

- [11] H. Tsunetsugu, T. Fujiwara, K. Ueda, and T. Tokihiro, “Electronic properties of the Penrose lattice. I. energy spectrum and wave functions,” *Physical Review B*, vol. 43, no. 11, p. 8879, 1991.
- [12] S. Martin, A. Hebard, A. Kortan, and F. Thiel, “Transport properties of Al₆₅Cu₁₅Co₂₀ and Al₇₀Ni₁₅Co₁₅ decagonal quasicrystals,” *Physical Review Letters*, vol. 67, no. 6, p. 719, 1991.
- [13] J.-M. Dubois, *Useful quasicrystals*. World Scientific, 2005.
- [14] S. Sakai, N. Takemori, A. Koga, and R. Arita, “Superconductivity on a quasiperiodic lattice: Extended-to-localized crossover of cooper pairs,” *Physical Review B*, vol. 95, no. 2, p. 024509, 2017.
- [15] K. Kamiya, T. Takeuchi, N. Kabeya, N. Wada, T. Ishimasa, A. Ochiai, K. Deguchi, K. Imura, and N. Sato, “Discovery of superconductivity in quasicrystal,” *Nature Communications*, vol. 9, no. 1, p. 154, 2018.
- [16] D. L. Sidebottom, *Fundamentals of Condensed Matter Crystalline Physics: An Introduction for Students of Physics and Materials Science*. Cambridge University Press, 2012.
- [17] M. Baake and U. Grimm, *Aperiodic Order*, vol. 1. Cambridge University Press, 2013.
- [18] W. Steurer, “Twenty years of structure research on quasicrystals. Part I. pentagonal, octagonal, decagonal and dodecagonal quasicrystals,” *Zeitschrift für Kristallographie-Crystalline Materials*, vol. 219, no. 7, pp. 391–446, 2004.
- [19] C. Janot, “Quasicrystals,” in *Neutron and Synchrotron Radiation for Condensed Matter Studies*, pp. 197–211, Springer, 1994.
- [20] L. Bindi, P. J. Steinhardt, N. Yao, and P. J. Lu, “Natural quasicrystals,” *Science*, vol. 324, no. 5932, pp. 1306–1309, 2009.
- [21] R. Penrose, “The role of aesthetics in pure and applied mathematical research,” *Bull. Inst. Math. Appl.*, vol. 10, pp. 266–271, 1974.
- [22] F. P. M. Beenker, *Algebraic theory of non-periodic tilings of the plane by two simple building blocks: a square and a rhombus*. Book by Eindhoven University of Technology Eindhoven, The Netherlands, 1982.
- [23] K. Jiang and P. Zhang, “Numerical methods for quasicrystals,” *Journal of Computational Physics*, vol. 256, pp. 428–440, 2014.

- [24] Y. E. Kraus, Y. Lahini, Z. Ringel, M. Verbin, and O. Zilberberg, “Topological states and adiabatic pumping in quasicrystals,” *Physical Review Letters*, vol. 109, no. 10, p. 106402, 2012.
- [25] O. Zilberberg, S. Huang, J. Guglielmon, M. Wang, K. P. Chen, Y. E. Kraus, and M. C. Rechtsman, “Photonic topological boundary pumping as a probe of 4D quantum hall physics,” *Nature*, vol. 553, no. 7686, p. 59, 2018.
- [26] J.-M. Gambaudo and P. Vignolo, “Brillouin zone labelling for quasicrystals,” *New Journal of Physics*, vol. 16, no. 4, p. 043013, 2014.
- [27] J.-N. Fuchs, R. Mosseri, and J. Vidal, “Landau levels in quasicrystals,” *arXiv preprint arXiv:1807.10032*, 2018.
- [28] G. G. Naumis and F. López-Rodríguez, “The electronic spectrum of a quasiperiodic potential: From the Hofstadter butterfly to the Fibonacci chain,” *Physica B: Condensed Matter*, vol. 403, no. 10-11, pp. 1755–1762, 2008.
- [29] B. Sutherland, “Self-similar ground-state wave function for electrons on a two-dimensional penrose lattice,” *Physical Review B*, vol. 34, no. 6, p. 3904, 1986.
- [30] M. Kohmoto and J. R. Banavar, “Quasiperiodic lattice: Electronic properties, phonon properties, and diffusion,” *Physical Review B*, vol. 34, no. 2, p. 563, 1986.
- [31] P. Kalugin and A. Katz, “Electrons in deterministic quasicrystalline potentials and hidden conserved quantities,” *Journal of Physics A: Mathematical and Theoretical*, vol. 47, no. 31, p. 315206, 2014.
- [32] N. Macé, A. Jagannathan, P. Kalugin, R. Mosseri, and F. Piéchon, “Critical eigenstates and their properties in one- and two-dimensional quasicrystals,” *Physical Review B*, vol. 96, no. 4, p. 045138, 2017.
- [33] J. Bellissard, “Gap labelling theorems for Schrödinger operators,” in *From number theory to physics*, pp. 538–630, Springer, 1992.
- [34] N. Mace, *Electronic properties of quasicrystals*. PhD thesis, Université Paris-Saclay, 2017.
- [35] N. Bédaride and T. Fernique, “The Ammann–Beenker Tilings Revisited,” in *Aperiodic Crystals*, pp. 59–65, Springer, 2013.

- [36] E. H. Lieb and F. Wu, “EH Lieb and FY Wu, Phys. Rev. Lett. 20, 1445 (1968).,” *Phys. Rev. Lett.*, vol. 20, p. 1445, 1968.
- [37] Y. Ovchinnikov and A. Larkin, “Nonuniform state of superconductors,” *Zh. Eksp. Teor. Fiz.*, vol. 47, p. 762, 1964.
- [38] P. Fulde and R. A. Ferrell, “Superconductivity in a strong spin-exchange field,” *Physical Review*, vol. 135, no. 3A, p. A550, 1964.
- [39] L. Baksmaty, H. Lu, C. Bolech, and H. Pu, “A Bogoliubov–de Gennes study of trapped spin-imbalanced unitary Fermi gases,” *New Journal of Physics*, vol. 13, no. 5, p. 055014, 2011.
- [40] L. Baksmaty, H. Lu, C. Bolech, and H. Pu, “Concomitant modulated superfluidity in polarized Fermi gases,” *Physical Review A*, vol. 83, no. 2, p. 023604, 2011.
- [41] T. Koponen, *Fermionic superfluidity in optical lattices*. PhD thesis, University of Jyväskylä Department of Physics, 2008.
- [42] C. Yang, W. Gao, and J. C. Meza, “On the convergence of the self-consistent field iteration for a class of nonlinear eigenvalue problems,” *SIAM Journal on Matrix Analysis and Applications*, vol. 30, no. 4, pp. 1773–1788, 2009.
- [43] C. G. Broyden, “A class of methods for solving nonlinear simultaneous equations,” *Mathematics of computation*, vol. 19, no. 92, pp. 577–593, 1965.
- [44] D. D. Johnson, “Modified Broydens method for accelerating convergence in self-consistent calculations,” *Physical Review B*, vol. 38, no. 18, p. 12807, 1988.
- [45] A. Baran, A. Bulgac, M. M. Forbes, G. Hagen, W. Nazarewicz, N. Schunck, and M. V. Stoitsov, “Broydens method in nuclear structure calculations,” *Physical Review C*, vol. 78, no. 1, p. 014318, 2008.
- [46] T. Koponen, T. Paananen, J.-P. Martikainen, and P. Törmä, “Finite-temperature phase diagram of a polarized Fermi gas in an optical lattice,” *Physical Review Letters*, vol. 99, no. 12, p. 120403, 2007.
- [47] T. Koponen, T. Paananen, J.-P. Martikainen, M. Bakhtiari, and P. Törmä, “FFLO state in 1-, 2-and 3-dimensional optical lattices combined with a non-uniform background potential,” *New Journal of Physics*, vol. 10, no. 4, p. 045014, 2008.

- [48] K.-E. Huhtinen, M. Tylutki, P. Kumar, T. I. Vanhala, S. Peotta, and P. Törmä, “Spin-imbalanced pairing and Fermi surface deformation in flat bands,” *Physical Review B*, vol. 97, no. 21, p. 214503, 2018.
- [49] J. Baarsma and P. Törmä, “Larkin-Ovchinnikov phases in two-dimensional square lattices,” *Journal of Modern Optics*, vol. 63, no. 18, pp. 1795–1804, 2016.

Appendix A

Appendix

Fibonacci chain

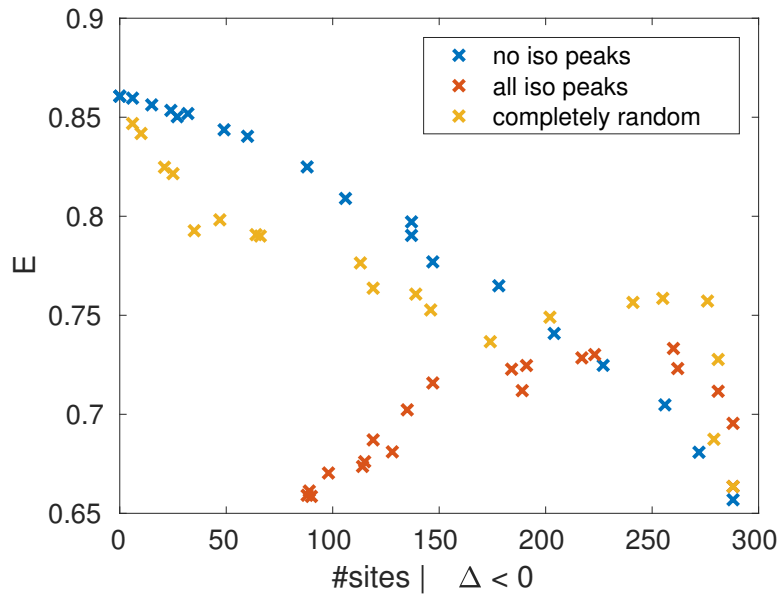


Figure A.1: The grand canonical energy as a function of number of sites where the order parameter is negative for Fibonacci chain of length $L = 377$. This chain has 88 isolated sites. These are the converged results of the iterations with three different initial ansatz for $U = -3t$, $T = 0.1t$, and $t_l = -0.53$. The three different ansatz include a completely random initial ansatz, an ansatz where a random amount of the non-isolated sites are set to negative values (*no iso peaks*), and an ansatz where all isolated sites are set to negative values and a random amount of non-isolated sites are set to negative values. The minimum of energy can be found when the order parameter is negative at all the isolated sites or its mirrored counterpart with order parameter positive at all of the isolated sites. This corresponds to the polarized BCS phase, with $\mu = 0$ and $h = 0.49$.

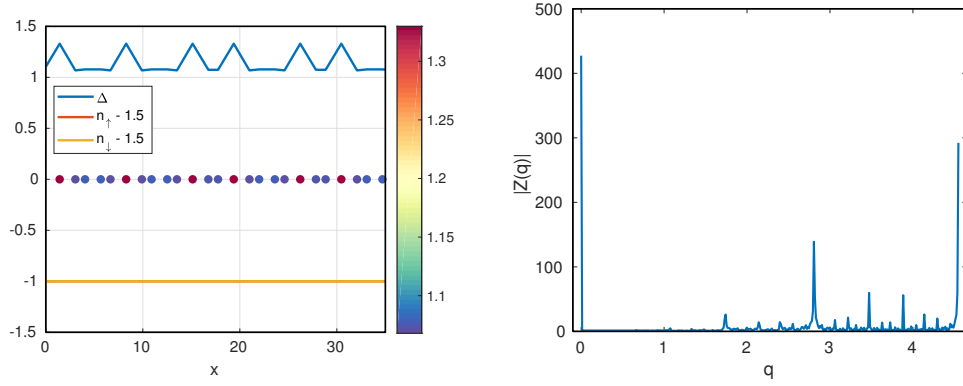


Figure A.2: Order parameter amplitudes for Fibonacci chain with $L = 377$ with periodic boundary conditions together with the Fourier transformation of the amplitudes. The interaction strength is $U = -3t$ and the temperature is $T = 0.1t$. The effective magnetic field $h = 0$ and average chemical potential is $\mu = 0$.

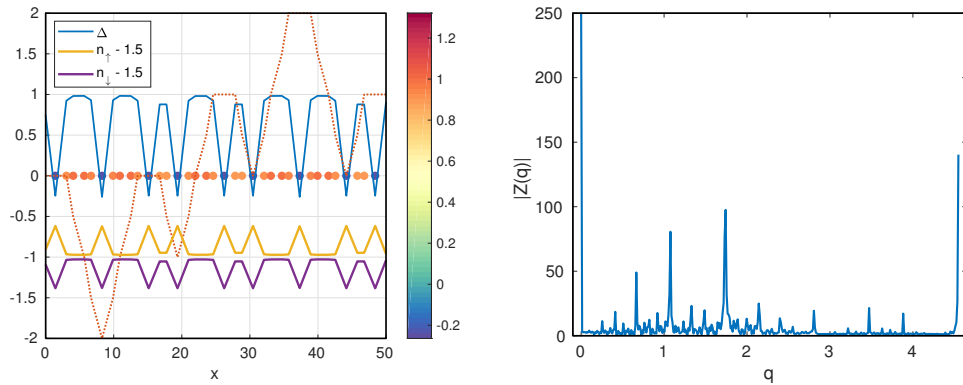


Figure A.3: Order parameter amplitudes for Fibonacci chain with $L = 377$ with periodic boundary conditions together with the Fourier transformation of the amplitudes. The interaction strength is $U = -3t$ and the temperature is $T = 0.1t$. The effective magnetic field $h = 0.69$ and average chemical potential is $\mu = 0$.

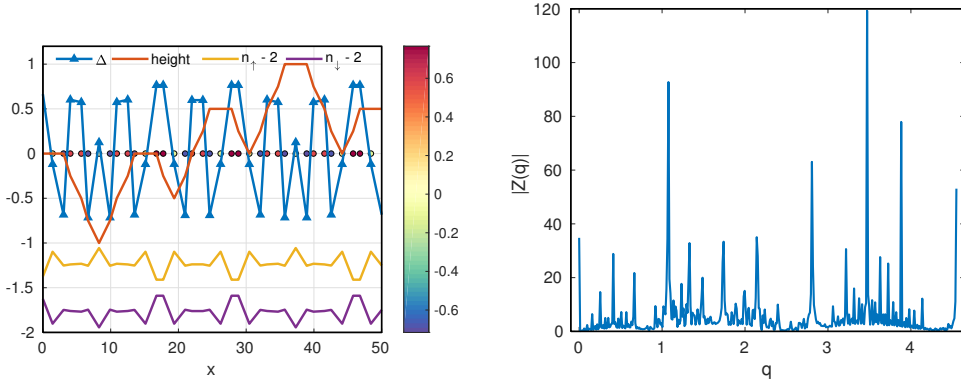


Figure A.4: Order parameter amplitudes for Fibonacci chain with $L = 377$ with periodic boundary conditions together with the Fourier transformation of the amplitudes. The interaction strength is $U = -3t$ and the temperature is $T = 0.1t$. The effective magnetic field $h = 1.05$ and average chemical potential is $\mu = 0$.

Ammann-Beenker tiling

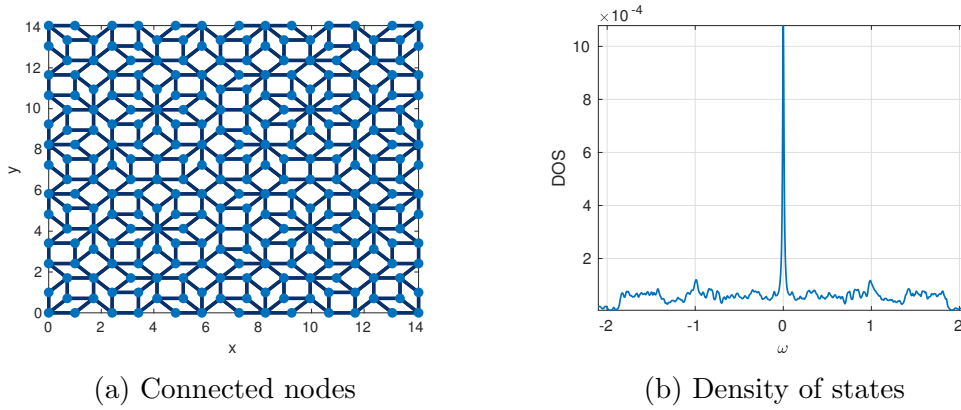


Figure A.5: a) The nearest neighbour connections of the Ammann-Beenker lattice with $N = 3$ inflations. The diagonals of the square tiles are not connected. b) The non-interacting density of states of the Ammann-Beenker lattice with $N = 5$ inflations, resulting in 8119 nodes.

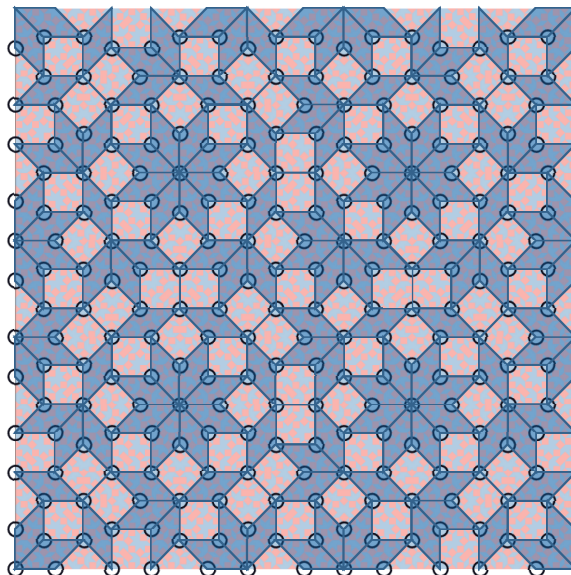


Figure A.6: Ammann-Beenker tiling with three inflations shown on top of the tiling with five inflations. The black circles denote the high-symmetry sites of the lattice inflated five times. These are the same as the nodes of the thrice inflated tiling.